An investigation into the weld integrity of the head-to-skirt junction on tall distillation columns

L. Brink
12091596

Dissertation submitted in partial fulfilment of the requirements for the degree *Master in Engineering* at the Potchefstroom campus of the North-West University

Supervisor: Prof. J. Markgraaff
Co-Supervisor: Dr. C. Nel

November 2010

Abstract

This study addresses the fatigue life of the head-to-skirt welds of tall distillation columns. Fatigue tests were done on two types of weld geometries which approximate the head-to-skirt configurations. From the fatigue tests it was determined that the fatigue life of the experimental samples can be substantially improved by applying weld build-up between the head and the skirt.

The expected fatigue life of the test samples was determined by way of calculation employing the so called Nominal-Stress-Approach, the Effective-Notch-Stress-Approach and the Stress-Life-Approach.

For both the Nominal-Stress-Approach and the Effective-Notch-Stress-Approach the predicted fatigue life was found to be overly conservative compared to the experimental results. The Stress-Life-Approach predicted the fatigue life to within a factor of 1.3 for both the geometries under investigation when displacements due to welding are taken into account. If displacements due to welding is omitted this factor is increased, for the geometry without weld build-up, to 2. For the geometry with weld build-up the factor remains 1.3.

Keywords: Fatigue test, fatigue life, head-to-skirt weld, pressure vessel support, weld, local weld geometry, Nominal-Stress-Approach, Effective-Notch-Stress-Approach, Stress-Life-Approach

Uittreksel

Die studie fokus op die vermoeidheidslewe van die sweisnaat tussen die kolom ondersteuning en kolom kop van hoë distallasie kolomme. Vermoeidheidstoetse is gedoen op twee geometrieë wat die sweisnaat geometrie benader. Uit die vermoeidheidstoetse is gevind dat die vermoeidheidslewe van die eksperimentele toetsstukke drasties verbeter kan word deur sweis-bottering tussen die ondersteuning en die kop van die kollom te doen.

Die verwagte vermoeidheidslewe van die toetsstukke is bereken deur middel van die Nominale-Spannings-Metode, die Effektiewe-Keep-Spannings-Metode en die Spannings-Lewe-Metode.

Vir beide die Nominale-Spannings-Metode en die Effektiewe-Keep-Spannings-Metode is die berekende vermoeidheidslewe as dit met eksperimentele resultate vergelyk word baie konserwatief. Die Spannings-Lewe-Metode voorspel die vermoeidheidslewe akkuraat tot ‘n faktor van 1.3 vir beide geometrieë as verplasings, van die sweisproses, inaggeneem word. As verplasings nie inaggeneem word nie raak die akkuraatheid van die lewensvoorspelling slegter en vermeerder die faktor tot 2 vir die geometrie sonder sweis-bottering. Vir die geometrie waar sweis-bottering gedoen is bly die faktor 1.3 al word die verplasings inaggeneem.

Sleutelwoorde: Vermoeidheidstoetse, vermoeidheidstoetse, kolom ondersteuning, sweis, lokale sweis geometrie, drukvat ondersteuning, Nominale-Spannings-Methode, Effektiewe-Keep-Spannings-Metode, Spannings-Lewe-Methode

Acknowledgements

I would like to thank Dr. Schalk Kok, of the CSIR, and Carl Coetzee, from Sasol, who assisted with the general formulation of the problem statement and for assisting with the gathering of the background information.

To Prof. Johan Markgraaff, thank you for the quick feedback each time and assistance. To Dr. Carl Nel, thank you for the technical assistance. I would not have been able to complete this work without your assistance and guidance.

Lastly thank you to my husband, Lukas and my parents for their continued support. Without your assistance and understanding I would not have persisted with this study.

Contents

List of Figures

List of Tables

1 Introduction

In the petrochemical industry use are often made of columns, for example in distillation processes. A distillation column is used to separate two products with different boiling points by introducing heat into the column. Due to the chemical process requirements these columns always have a high height to diameter ratio. These height to diameter ratios have increased dramatically over the last few years. Proof of this is that the tallest column in the southern hemisphere was recently constructed for Sasol in Secunda.

Table 1-1 presents operating parameters and dimensions of some recently constructed columns at Sasol, Sasolburg (Sasol Project Document, 2008; Sasol Project Document, 2010). According to the Occupational Health and Safety act of South Africa (Department of Labor, 2008), Vessels under Pressure Regulation a vessel is rated as a pressure vessel if all of the following criteria apply. The fluid is above its boiling point at atmospheric pressure. The capacity in cubic meters times the pressure in pascal is more than 15000. The design pressure of the vessel is more than 40 kPa and the nominal inside diameter of the vessel is more than 150 mm.

From Table 1-1 it can be concluded that the dimensions of the columns and the internal pressure of the columns will always quantify the column as a pressure vessel and therefore must be designed and constructed in accordance with an acceptable code.

Table 1-1 Typical operating parameters and dimensions of columns manufactured and constructed at Sasol, Sasolburg.

Pressure Bar	Temperature °C	Length m	Diameter m	L/D Ratio
4	130	44.3	1.9	23
4	165	16	0.92	17
4	195	51.6	1.6	32
24	50	60.15	3	20
21	65	39.2	2.4	16
4	65	7.04	1	7

Figure 1-1 shows a schematic representation of a typical distillation column. This illustrates that the column typically consist of an external shell, two 2:1 ellipsoidal heads, various nozzles, a skirt as support, and internals.

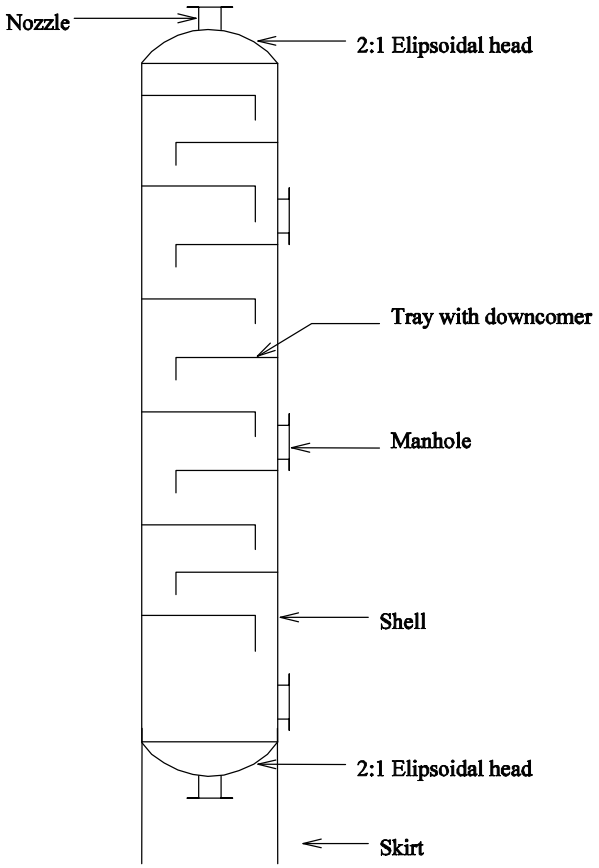

Figure 1-1: Schematic representation of a section through a typical distillation column

Historically the head-to-skirt welds were made as shown in Figure 1-2 (Sasol Standard 4001E, 1988). For length to diameter ratios below 12[(1)] the welding is only done from the outside, with no gap between the head and skirt (Figure 1-2a). This creates a large stress concentration between the head and skirt of the vessel due to the small angle between the contact surfaces. Where the length to diameter ratio exceeds 12 the configuration as shown in Figure 1-2b was used. In this case the welding is also only done from the outside, but with a 3 mm root gap between the head and skirt to reduce the edge-on-edge

contract stress. It is claimed that this weld design allows for better penetration between the head and skirt and provides a bigger angle at the root of the weld reducing inferred stresses between the contact surfaces.

On the two weld configurations shown in Figure 1-2 the only non-destructive testing that can be done, on these welds, is dye-penetrant testing or magnetic-particle testing that can only detect surface defects. Due to the weld configuration no ultrasonic testing or radiographic testing to ensure absence of internal defects can be carried. It was though that undetected internal defects can be present in these welds that can give

Foot note:

(1) It was found that, for the wind speeds given in ASCE 7/02, 2nd Edition, Minimum Design Loads for Building and Other Structures, the length to diameter ratio of 12 is the critical transition point.

rise to stress points leading to weld failure.

As the columns height to diameter ratio increase the stress in the head-to-skirt weld increase and therefore the possible stress concentrations present in the weld becomes more of a concern.

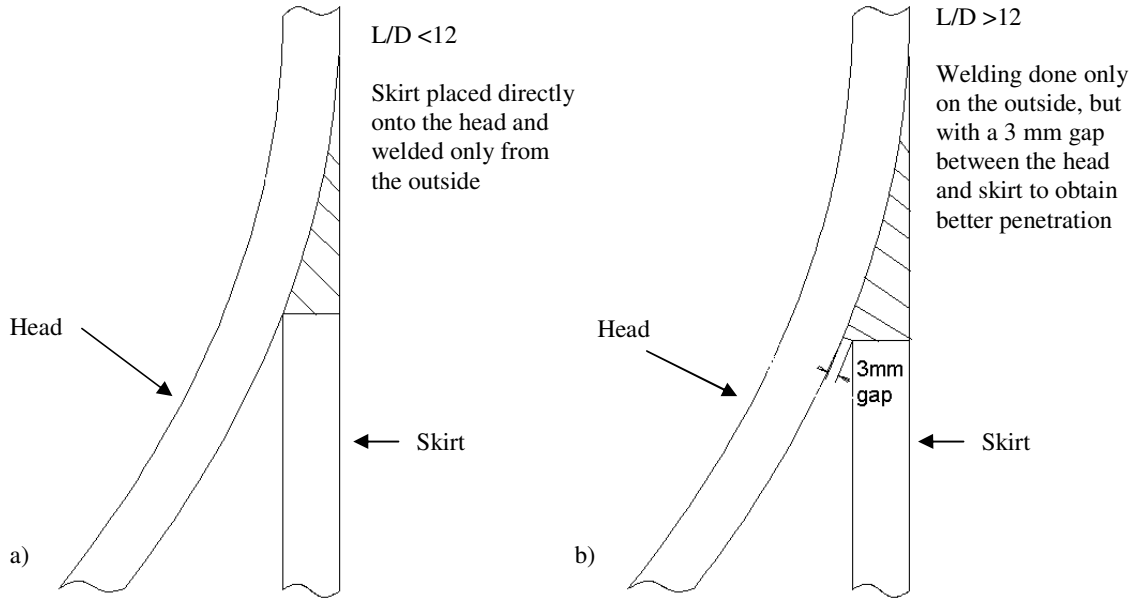

Figure 1-2: Representation of the historic weld configuration used to weld the head-to-skirt of vertical pressure vessels constructed for Sasol

1.1 Problem statement

With an increase in length to diameter ratios, vibration problems due to dynamic wind loading are in addition also experienced. A good example of a dynamic wind loading problem which took place at the Sasol plant in Secunda, occurred when one of the columns that was empty, was excited at its natural frequency due to vortex shedding (Coetzee, 2005). Because of the oscillation of the column, failures were experienced at the head-to-skirt weld contact surfaces of this column (Coetzee, 2005). This necessitated an investigation into optimum length to diameter ratios that can accommodate vortex shedding as well as the identification of contact weld configurations prone to failure.

The investigation concluded that extra requirements, such as vortex shedding calculations, fatigue finishing of welds in certain sections of columns and different head-to-skirt weld configurations, are required on all newly constructed columns where the length to diameter ratio exceed the value of 12.

The weld configuration shown in Figure 1-3b has since been implemented (Figure 1-3b, Sasol Standard 4001E, 2008). This weld configuration was chosen to lessen the stress concentration of the weld and to allow it to be checked for defects by ultrasonic examination. The main requirements specified for the weld configuration are that an inside radius of more than 5 mm between the head and skirt, obtained through weld build-up, is required in order for center lines to meet and that ultrasonic testing must be possible. All though this modification was intended to reduce the risk of weld failures it may also result in an increase in residual stresses and distortions in the shell (Maddox, 1991; Coetzee, 2005).

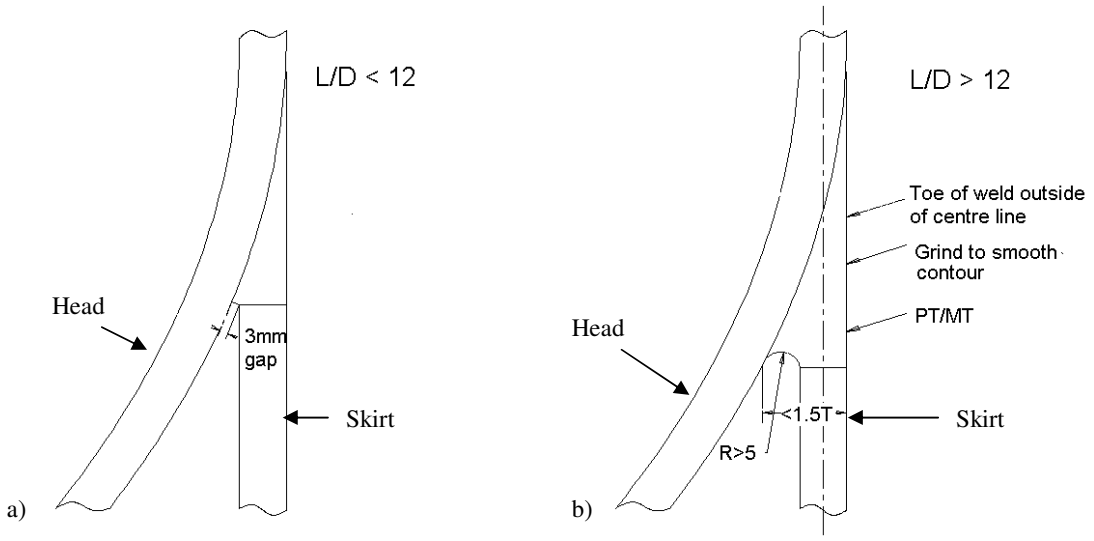

Figure 1-3: Representation of the new configuration used to weld the head-to-skirt of vertical pressure vessel constructed for Sasol

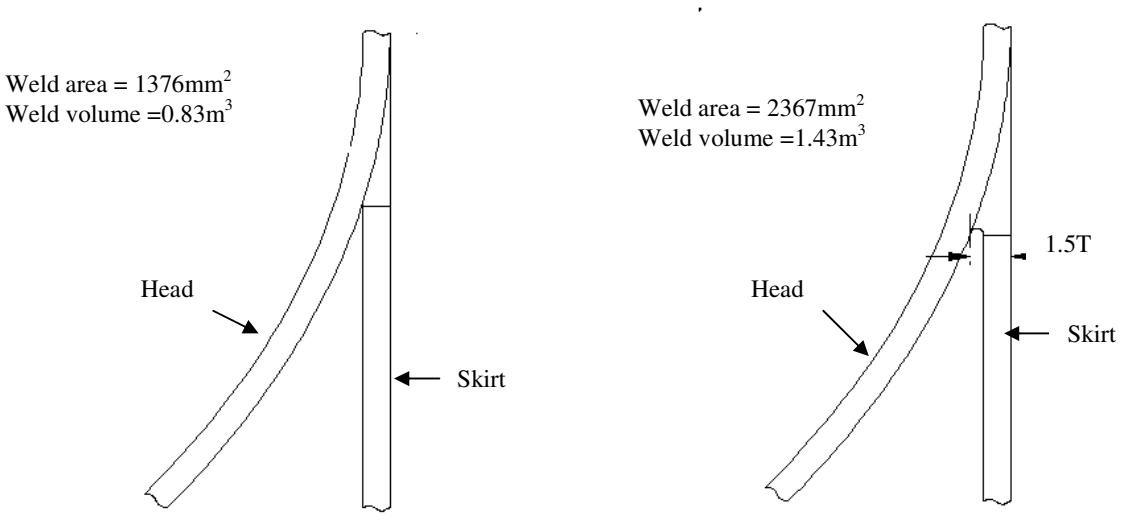

a) Weld configuration without weld build-up as in Figure 1-3a.

a) Weld configuration with weld build-up as in Figure 1-3b.

Figure 1-4: Difference in the amount of welding required between the two head-to-skirt configurations

Figure 1.4 shows the difference between the amount of welding for two configurations on a 1.9 m diameter column with a wall thickness of 25 mm. This illustrated that the weld volume increased by 72%

from the configuration *without* weld build-up (Figure 1-4a), to the one with weld build-up (Figure 1-4b), which also increases cost.

However, of greater concern is the possible increase in residual stresses and displacement in the shell (Coetzee, 2005). The high amount of welding can cause the shell to deform to such an extent that the dimensional tolerances allowed by the code of construction, for instance ASME VIII Div.1 are no longer met. This is especially true on thin-walled vessels and vessels manufactured from stainless steel. (Coetzee, 2005)

The new dimensions as shown in Figure 1-3b were chosen based on the ASME VIII Div. 1 requirements for tall distillation columns as well as Sasol experience. However, as ASME VIII Div. 1 does not cover actual dimensional requirements, the question arises as to whether the suggested radius of the head-to-skirt weld is truly required, and whether this can be decreased to reduce possible residual stresses created in the pressure vessel heads. Some manufacturers also proposed to rather use GTAW (Gas Tungsten Arc Welding) to melt back the root. This proved to improve fatigue life (Maddox & Manteghi, 2004:2; Hobbacher, 2004: 87) and it is claimed to cause less residual stress and distortion.

This study focuses on whether the modified dimensions of the adopted weld configuration will indeed improve fatigue life and if GTAW re-melting would suffice.

2 Literature study

This chapter focuses on the legal requirements that are applicable to the tall distillation columns under investigation and presents the findings of a literature study on the head-to-skirt welds and associated problems that are of value to resolving the problem statement and provide background information.

2.1 Regulatory requirements

2.1.1 Occupational Health and Safety Act

All equipment used in South Africa regardless of the industries concerned, must comply with the Occupational Health and Safety Act of South Africa (85/1993). This consists of various sections of which the Vessels under Pressure Regulation is one of these sections. According to this regulation, Section 1, all vessels are classified as pressure vessels unless one of the following applies. (Department of Labor, 2008)

- The vessel is a boiler.
- The boiling point of the liquid in the vessel is not exceeded at atmospheric pressure and no gas can form on top of the liquid in the vessel.
- The vessel is a working cylinder or chamber of a steam, heat or air engine.
- The vessel is an integral operating part of a motor vehicle or locomotive.
- The vessel is a portable gas container.
- The design pressure in pascal multiplied by the capacity in cubic meters is less than 15000.
- The design pressure of the vessel is below 40 kPa.
- The vessel has a nominal inside diameter of less than 150 mm.
- The vessel is a hand held fire extinguisher.

Table 1-1 (Chapter 1) shows the typical pressures, temperatures and dimensions of the columns under investigation. This clearly shows that even though the columns have different design pressures and dimensions it will always be classified as pressure vessels. The South African law therefore requires the columns to be designed and manufactured in accordance with one of the codes recognized by the Vessel under Pressure Regulation. This includes design and construction according to ASME VIII Div. 1 (American Society of Mechanical Engineers) Unfired Pressure Vessels. This is the most commonly used specification on Sasol plants and therefore this section focuses on the ASME VIII Div.1. requirements for the head-to-skirt junction.

2.1.2 ASME Code requirements

2.1.2.1 ASME VIII Div. 1

This study used ASME VIII Div 1, 2007 (ASME, 2008a) to determine the design criteria for the head-to-skirt junction on a vessel.

Section UG governs the materials than can be used for the head (UG-4 to UG-15) as well as the wall thickness calculations (UG-21 and UG-32), however no mention is made of methods to calculate skirt thickness. Similarly, Section UW gives guidelines on the weld design of the pressure-containing parts, like the head to shell junction and the nozzle to shell joints. In ASME VIII Div. 1 the typical weld configurations are divided into Weld Categories A, B, C and D as shown in Figure 2-1 (ASME, 2008a). Each of these weld categories then give guidelines to the static design criteria as well as the non-destructive testing to be carried out on each of the welds. Since no support configurations is shown in Figure 2-1 the head-to-skirt junction is not governed by ASME VIII Div 1 as to weld design or NDE requirements. However section UW 28(b) clearly states that a Welding Procedure Specification (WPS) needs to be qualified in accordance with ASME IX for load-bearing attachments welded to pressure parts and UW-29(a) states that the welder must be qualified in accordance with ASME IX. Therefore, even though no clear indication is given on weld design i.e. size and NDE requirements, all welding must still conform to ASME IX.

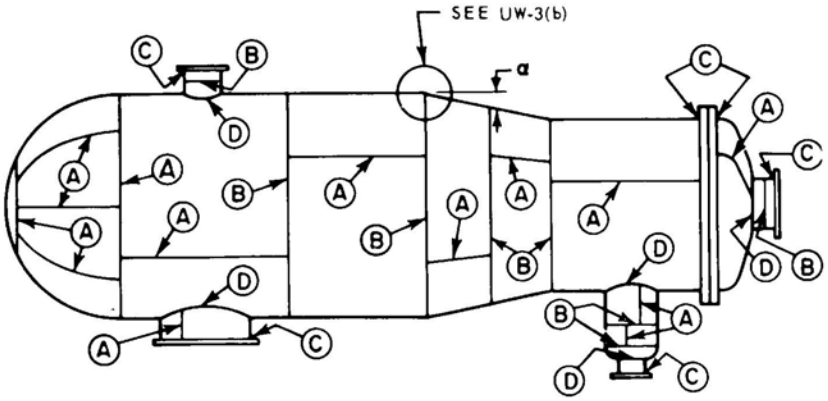

Figure 2-1: Weld configuration covered by ASME VIII Div.1 section UW. Ballooned symbols refer to weld types

ASME VIII Div. 1 does however contain a non-mandatory Appendix, Appendix G, entitled Suggested Good Practice Regarding Piping Reactions and Design of Supports and Attachments, which gives some guidelines on what should be considered during the design of these types of supports.

Section G-1 simply states that it is recognized that at vessel supports concentrated loads will be present that can cause primary and secondary stresses in the vessel shell higher than that designed for during internal pressure calculations, however no design calculation requirements are given due to various factors which may influence the design. While section G-2 states that the details of the supports should conform to good structural practice, it provides some guidelines on what to consider.

Section G-5 gives some guidelines for large and heavy vertical vessels supported on skirts. The columns under investigation fall into this category. The following is a summary of the guidelines:

- The best location for the line of skirt attachment should be determined by taking into account loading during hydrostatic testing as well as for any load combination at the highest expected metal temperature at normal operating pressure.
- When applying loads to the vessel and skirt, the skirt reaction must be considered in addition to the pressure effects. This includes the compression on the head and skirt due to the weight of the vessel and contents above the weld, the effect of the weight below the weld on the head and skirt and the load applied due to wind and other external loads.
- In most cases the mean diameter of the skirt and shell should be approximately the same and the head should have a generous knuckle radius to ensure that localized stresses are minimized. In some cases however it would be warranted to investigate the dimensions more thoroughly.

2.1.2.2. ASME IX

The requirements for the pressure vessel welds as stipulated in ASME IX (ASME, 2008b) can be summarized as follows:

From part QW the following is specified for all production welds to be done. A Welding Procedure Specification (WPS) must be drawn-up for each weld to be carried out. This WPS is required to give the welder directions on the weld character to be completed and to ensure code compliance. The WPS must list all essential, non-essential and supplementary essential variables, if required.

Essential variables on the WPS are those variables which when changed, are expected to affect the mechanical properties of the weld. Non-essential variables are those variables which do not affect the mechanical properties of the weld if changed. Supplementary essential variables are treated as non-essential, unless notch toughness tests are required, when they become essential variables.

For each WPS there must be an approved Procedure Qualification Record (PQR) and this must be referenced on the WPS. The PQR is a record of the welding variables during the welding of a test coupon. It also contains the records of the tests done to prove the strength of the weld. These tests are typically bend, tensile and macros as required. The PQR must contain all essential variables and supplementary essential variables if required. It may contain the non-essential variables; however only variables measured should be recorded. If a variable was not measured, it should not be recorded. More than one procedure can be qualified on a test coupon. Any change on the PQR except editorial changes, requires re-certification of the PQR by means of testing.

What should be noted though is that the WPS and PQR qualified in accordance with AMSE IX only determine that the proposed weld for construction is capable of having the required properties for its application. It does not guarantee that the production weld will be without defects.

For all production welds a qualified welder must be used. A welder is qualified by testing his/her ability to deposit sound weld metal. A welder must be qualified for each procedure i.e. GTAW (Gas Tungsten Arc Welding), SMAW (Shield Metal Arc Welding). All essential variables must be recorded during the welding of the test piece. The test piece is then tested either by radiographic testing or mechanical bend tests. If the welder passes he/she is qualified for the procedure within the limits allowed for by the specific table. All welders must be re-qualified every six months, however if they have been welding production welds on that specific process, this is not required.

2.1.2.3 Conclusion

In conclusion, ASME VIII Div. 1 does not give guidelines on how the head-to-skirt junction configuration should be designed, except that the center line of the head and the skirt should preferably coincide. However ASME IX does detail that the weld should be made with a qualified welding procedure by a qualified welder.

Good engineering practice does however require that the head-to-skirt weld meets some minimum requirements to ensure that the pressure vessels are safe to operate. Therefore other methods of determining the required weld geometry must be investigated, and this must include static as well as fatigue loading.

2.2 Literature

Literature searches could not provide any results on research carried out on weld and weld configurations of head-to-skirt junctions of tall columns. Publications from the International Institute of Welding (IIW)

were searched as well the ASME code cases and no specific mention of such weld configuration could be found. The focus then shifted to reviewing the basic principles of weld design, which include static design, fatigue design and residual stresses and distortions to gain more insight and in order to further approach the problem.

2.3 Static design

For static strength design a specific geometry is chosen, which is then modeled on a finite element model. Load conditions taken into account for such finite element modeling are maximum design pressure, wind loading typically obtained from the Sasol Specifications and weight, for a empty and a full vessel. The stresses obtained are then verified against the ASME VIII Div 1 allowable stresses. If the stresses obtained from the finite element method are found to be lower than the allowable value specified in ASME VIII Div 1 the presented weld geometry is accepted in terms of static strength. What should be noted is that this method only focuses on the specific weld geometry and that all displacement and residual stresses due to welding, are ignored. Figure 2-2 shows the typical stress distribution in the head-to-skirt junction and weld region of the Replacement Alcohol Water Splitter Column of the Sasol Plant in Secunda, obtained by a finite element analysis (Turnmill Proquip, 2006).

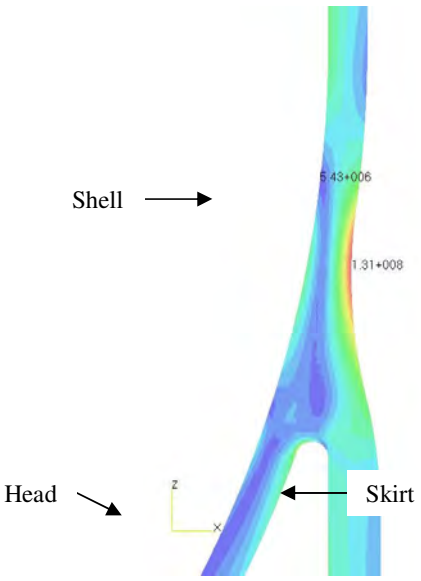

Figure 2-2: Typical stress distribution results for static head-to-skirt junction design (Modified after Turnmill Proquip report). Red zone represent the highest stress zone.

2.4 Fatigue design

Even though the head-to-skirt junction on a pressure vessel does not seem to have been researched before in detail, the fatigue of weld design is an active research field.

As described in a study by Radaj (1996), when looking at the fatigue design of a welded joint, various factors needs to be taken into account. Among these the geometry of the weld, the metallurgical changes in the area of the weld due to heating and cooling, introduction of residual stresses and inhomogeneous material properties due to filler metal, are applicable. However, Radaj (1996) found that these parameters remain largely unconsidered in local approaches used for predicting failure of welds due to fatigue.

From the literature reviewed it is conducted that in general, material characteristics of the base material are used to predict the fatigue strength of the weld as properties for the filler metal and heat-affected zone (HAZ) are difficult to obtain. This despite the fact that fatigue failures of welds are mostly experienced in the HAZ. The residual stresses present in welds can be as large as the yield strength of the material, which influence the fatigue life of the welds, but are still disregarded or only roughly taken into account. Lastly the actual weld geometries that are produced in the workshops have varying dimensions, which also influence the fatigue life of the welds.

The following section explores how the variables influence the fatigue life.

2.4.1 General considerations

2.4.1.1. Geometry of the weld

In both fillet and butt welds the weld causes a stress concentration which, if ignored, can lead to non-conservative life predictions if based on calculations. As described by Teng *et al*. (2002) the severity of the stress concentration will depend on the weld geometry i.e. the flank angle (θ), weld toe radius (r) and edge preparation angle (Φ). These parameters are shown in Figure 2.3. They found that a decrease in flank angle or increase in weld toe radius increased the fatigue life by 51% and 21% respectively at 1.1 x 10^5 cycles due to the reduction in stress concentration factor. A further improvement of 6% in fatigue life at 1.1 x 10^5 cycles was found by decreasing the edge preparation angle due to the lower residual stresses that are created in this manner.

These factors are highly variable as they depend on the welding process used, the material being welded, the alignment of the elements to be joined and the skill of the welder (Radaj, 1996).

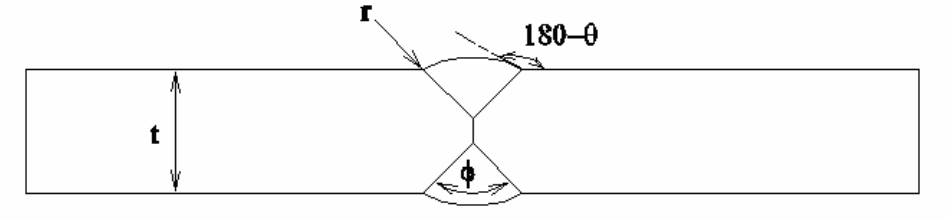

Figure 2-3: Geometric Weld parameters that influence the weld geometry

Other geometrical defects that can also influence the strength of the weld are cracks, pores, cavities, lack of fusion, overlap and inadequate penetration. However in ASME VIII Div 1 there are clear limits for acceptance of these defects. The influence of these defects is however, not considered as part of this study.

2.4.1.2 Residual stresses and displacement

Different types of welding techniques can be used to join plates. However, this study will only focus on arc welding, because it is the method most generally employed. Arc welding uses a heat source that creates an intense heat-input at one point. Due to this intense concentration of heat the regions near the weld line undergo severe thermal cycles, which result in inhomogeneous plastic deformation and residual stresses in the welded joint.

These residual stresses can be detrimental to the performance of the welded product. As discussed by Teng *et al*. (2002), Murugan *et al.* (2001) and Cheng *et al.* (2003) a tensile residual stress causes the structure to be more susceptible to fatigue damage, stress corrosion cracking and fracture. The stress condition in the welded area is therefore a function of the weld residual stresses and the applied stresses due to load.

The severity of the residual stresses obtained in the structure depends on the thermal input and the constraints imposed on the work piece. If the sides of the work piece are not constrained, lower residual stresses will occur as the structure is free to expand and contract at will during fusion. It will however increase the deformation of the structure. On the other hand, if the structure is not allowed to move, the induced stresses cannot redistribute and gives rise to higher residual stresses.

Even though there are methods to reduce residual stresses in a structure and improve fatigue life such as grinding, peening and GTAW re-melting, these in general only reduce the residual stresses or improve the weld profile by reducing sharp corners (Maddox & Manteghi, 2004:1). They do not eliminate the residual stresses, and should therefore still be considered in any analysis.

2.4.1.3 Material composition of the weld

In arc welding processes a filler metal is generally added to the weld pool. This filler metal is of similar composition as the base metal, but is specially alloyed to achieve the correct metallurgical structure, weld-pool shape, and improve droplet transfer and reduction of hot cracking (Radaj, 1996).

During the welding process the filler metal mixes with the base metal creating a new metallurgical composition. The high temperature also creates a change in microstructure and grain size in areas close to the weld which are heated to a sufficient temperature. This is accompanied by a change in the hardness values, yield strengths and crack propagation resistance due to transformation during cooling (Du Toit, 2004).

2.4.2 Fatigue approaches to welded structures

The three most commonly used fatigue prediction methods in welded joints are the *Nominal-Stress-Approach,* the *Hot-Spot-Stress-Approach* and the *Effective-Notch-Stress-Approach* (Hobbacher, 2004; Niemi, 1995; Niemi & Marquis, 2003). These approaches use different methods to predict the fatigue life of welded joints. Another approach, based more on first principle design, is the *stress-life-relationship* from Shigley (2001). These approaches are reviewed below.

2.4.2.1 Nominal-Stress-Approach

The Nominal-Stress-Approach makes use of weld categories, for instance a butt weld or fillet weld, and each weld category has a certain fatigue curve associated with it. For this study the methodology from Hobbacher (2004: 44) is reviewed.

According to this method the fatigue curves are identified by the characteristic fatigue strength for the specific weld category, at 2 million cycles, which is called the fatigue class (FAT). The slope of the curve for the weld details is m = 3, below 1 x 10^7 cycles and m = 22 above 1x10^7 cycles. See Figure 2-4 for a schematic representation of three of these fatigue classes. For instance a transverse loaded butt weld ground flush to the plate, with 100% Non destructive testing done will correspond to a FAT of 100 in steel.

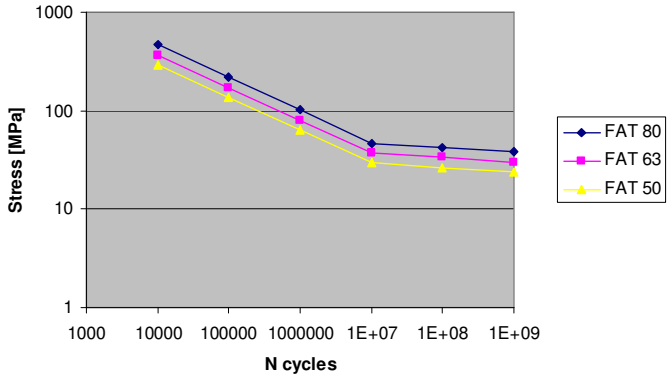

Figure 2-4: Fatigue resistance S-N curves for steel, based on the maximum principle stress range. The specific weld geometry will refer to a specific fatigue class (FAT).

The fatigue curves given in Hobbacher (2004: 47-74) are based on various samples with the same weld geometry. For instance one of the SN curves will be for a T-joint full penetration weld with the weld toes ground, while another will be for a T-joint without the weld toes ground. To determine these curves, various samples with different base metal thickness, different weld sizes and different local weld dimensions, as defined below, were tested.

As these fatigue curves are based on representative experimental data the following effects are included in the fatigue curves and do not need to be taken into when calculating the stress range:

1. Structural stress concentrations like misalignment, within the limits given in the fatigue class, due to the weld type shown.
2. The different local weld dimensions i.e. different weld toe radii, flank angles and edge preparation angles as these varied for the samples tested.
3. Local stress concentration due to the weld geometry and different sizes of the welds.
4. Weld imperfection consistent with normal fabrication standards.
5. Stress direction in the sample due to the type of loading applied.
6. Residual stresses created due to welding of the sample.
7. Metallurgical changes due to welding.
8. The type of welding process, normally fusion welding.
9. If an inspection procedure is specified this is included.
10. If post weld heat treatment is specified this is include.

The fatigue curves given are independent of the tensile strength of the materials, but are limited by the static strength of the material. The stress used to determine the fatigue life of the samples is the maximum principle stress range in the section where potential fatigue cracking is expected. This stress is calculated by only taking the nominal stress into account and not the stress concentration created by the actual weld.

However if a macro geometric stress concentration such as a hole is present in the geometry or more misalignment, as allowed by the weld fatigue class, these must be taken into account when determining the stress range.

2.4.2.2 Hot-Spot-Stress-Approach

The Hot-Spot-Stress-Approach is similar to the Nominal-Stress-Approach. Again the different weld geometries are divided into different fatigue classes. However for the Hot-Spot-Stress-Approach the fatigue classes are based on the hot spot stress calculated at the weld toe and not the nominal stress.

The fatigue classes as given in Hobbacher (2004:78), do not take the macro geometrical stress concentrations, such as misalignment into account and these considerations must be included when calculating the hot spot stress. However local weld geometries such as weld toe radius, edge preparation angle and flank angle were taken into account when the SN curves were developed and should therefore not be considered when the hot spot stress is calculated (Niemi & Marquis, 2003: 19).

2.4.2.3 Effective-Notch-Stress-Approach

The Effective-Notch-Stress-Approach, as described by Hobbacher (2004:80), uses one fatigue curve with the stress at two million cycles equal to 225MPa, for all steel sections. The same slopes as described in the Nominal-Stress-Approach are applied. However, for this approach the local highest notch stress at the point where failure is expected to occur is used to determine the principle stress range.

The local notch stress, δ_{ln}, is the highest stress located at the root of a notch, such as a weld toe. It includes the nonlinear stress peak obtained at the surface, thus implying that surface defects are more damaging than embedded defects. This stress is usually obtained from a linear-elastic FEM where the real weld contour is replaced by an effective one to take the statistical nature and scatter of weld shape parameters into account. According to Hobbacher (2004:80), it was found that for structural steels an effective notch root radius of 1 mm gave consistent results. Figure 2-5 shows an example of how this 1 mm radius is applied to the weld toes and roots of a butt weld and fillet weld.

This effective notch stress method is restricted to:

1. Welds where failure is expected from the weld toe or root.
2. Welds in the as-welded condition. If the weld has been ground or machined the actual dimensions of the weld should be modeled.
3. Welded plates with a wall thickness larger than 5 mm.

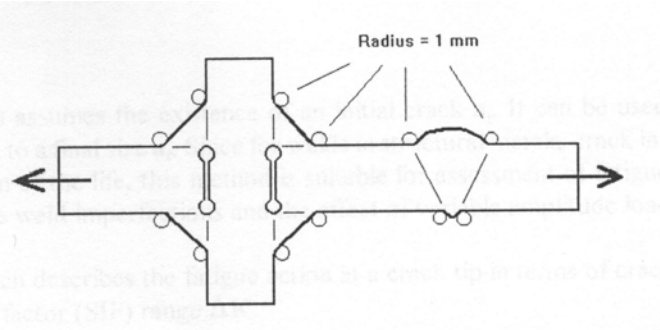

Figure 2-5: Typical weld root radii (1mm) as used in the Notch-Stress-Approach, as suggested by Hobbacher.

The flank angles that should be used in the FEM analysis are: 30° for butt welds and 45° for fillet welds, unless otherwise specified.

What should be noted is that, as the SN curve is based on experimental data, the residual stresses present in the weld area are implicitly taken into account. However any misalignment between the welded plates as well as macro geometric stress concentrations are not taken into account implicitly and must be modeled in the finite element analysis when determining the notch stress (Hobbacher, 2004:80).

2.4.2.4 Stress-Life-Approach

Another approach, based on first principles, which can be used to determine the fatigue life of welded samples is the *Stress-Life-Approach* as described in Shigley (2001:367). In this approach the fatigue life is calculated by means of the Basquin relation,

$$\delta_A = \delta'_F(2N)^b \quad (1)$$

with δ_A = the maximum stress amplitude,
δ'_F = the fatigue strength coefficient,
b = the fatigue strength exponent,
2N = the fatigue life,

In which the endurance limit (S_e) of the material, with endurance limit modifying factors are used. The endurance limit modifying factors that can be taken into account are k_a, surface finishing, k_b, size modification, k_c, load modification, k_d, temperature modification and k_e, miscellaneous effects.

The stress used to determine the fatigue life of the samples is the maximum principle stress amplitude multiplied by the fatigue stress concentration factor, K_f. The fatigue stress concentration factor is then given by:

$$K_f = \frac{K_t}{1 + \frac{2}{\sqrt{r}} \frac{K_t - 1}{K_t} \sqrt{a}} \tag{2}$$

with K_f = the fatigue stress concentration factor,

r = the radius of the stress concentration in the geometry

K_t = the static stress concentration factor

$\sqrt{a}$ = Heywood's Parameter.

Heywood's Parameter is determined based on the type of macro geometrical stress concentration present and is adjusted by the ultimate strength of the materials.

2.4.2.5 Conclusion

In conclusion, in the Nominal-Stress and Hot-Spot-Stress-Approaches generic fatigue curves are used, which do not take the local weld geometry into account. As this study focuses on how the local weld geometry influences the fatigue life of a specific weld the use of these approaches are generally unsuitable. Furthermore, these approaches are limited to weld geometries for which a fatigue curves exist. New weld geometries can be related to these curves, but it is thought that such an approach will not necessarily yield accurate results. It is however an easy and effective method to obtain the fatigue life of standard weld geometries, as residual stresses and material properties are implicitly taken into account.

With the Effective-Notch-Stress-Approach the local geometry of the weld is taken into account when calculating the fatigue life. This approach can therefore differentiate between similar weld geometries, such as the head-to-skirt junction, but with different local weld dimensions as described in Section 2.4.1.1.

Lastly for the Stress-Life-Approach the local stress concentration factor is taken into account when calculating the stress at the weld. Therefore similarly to the Effective-Notch-Stress-Approach, this approach will be able to distinguish between similar weld geometries, but with different weld dimensions.

2.4.3 Residual stresses and distortions created during welding

Residual stresses created during welding have an influence on the fatigue life of the welds. Even though the residual stresses can be obtained by welding samples or doing weld simulations, this is not generally

done when manufacturing a column. Furthermore, the range of parameters allowed by the WPS used by the manufacturers will create different residual stresses in each sample. It is therefore advisable that fatigue approaches which take residual stresses implicitly into account, be used.

Similarly, distortions will influence the geometry of the weld and therefore the fatigue life. Distortions can also cause the out of roundness of the vessels to go outside the ranges allowed by the codes and user specifications. Therefore this should be kept in mind when designing a weld.

Lindgren *et al.* (2001) gives a complete description of how thermal weld modeling can be done to predict the residual stresses and distortions created during the welding processes. However, this is not done in industry as the welding engineer normally does not have the expertise to do thermal weld modeling and the results obtained would be questionable. This is clearly illustrated in the study by Dong *et al.* (2002) whose findings showed that there were significant differences in the predicted temperature distributions and residual stresses when a specific problem was sent out to researchers in this field.

Even though residual stresses do have a significant effect on the fatigue life of welds, the fatigue approaches discussed in Section 2.4.2 implicitly take these into account. Therefore this study will not focus on thermal weld modeling to predict residual stresses.

3 Objective of the study

3.1 Introduction

From section 2.1.2 it should be clear that there are no code requirements for the head-to-skirt junction of a pressure vessel except that an approved WPS and PQR must be used and that a qualified welder is to carry out the welding. Furthermore, no papers were found of tall columns which specifically address the weld configuration the head-to-skirt junctions. Thus, good engineering practice based on basic principles need to be used to evaluate these types of junctions.

The static design of the weld can be done by means of a linear elastic finite element model, however from Section 1.1 it is evident that static strength is not the main concern. What should be determined is how the weld geometry influences fatigue life, taking into account residual stresses and displacement, and also manufacturing costs.

The following questions must be answered to determine this:

1. To what extend does the modified weld geometry as shown in Figure 1-3b, influence the fatigue life of a head-to-skirt welded joint?
2. What commonly used practical fatigue prediction methods can distinguish between the different weld geometries and to what extend can the life be predicted by these prediction methods and,
3. To note displacements and to investigate the possible influence on the integrity and the fatigue life of the weld.

3.2 Approach

The approach that was followed for this study is divided into the following phases:

Phase 1: Manufacturing of weld samples with two different geometries, while recording weld parameters such as potential difference, current and weld speed.
Phase 2: Conducting fatigue tests to establish whether there is a difference in fatigue life between the two geometries of concern.
Phase 3: Predicting the fatigue life of samples by means of the *Nominal-Stress-Approach*, the *Effective-Notch-Stress-Approach* and the *Stress-Life-Approach.*
Phase 4: Comparison of the predicted fatigue life (phase 3) and the experimentally obtained fatigue life.

4 Manufacturing of fatigue samples

4.1 Introduction

4.1.1 Sample geometry

The Sasol Standard drawing, for the head-to-skirt weld on tall columns, as shown in Figure 1-3, provides the specific geometries with which a head-to-skirt weld for various columns must comply. The actual dimensions of the weld however depend on the wall thickness of the skirt and head, as well as the diameter of the vessel.

Figure 4-1 shows the head-to-skirt welds for a column with a diameter of 1.9 m, head thickness of 25 mm and skirt thickness of 25 mm. Figure 4-1(a) shows the modified head-to-skirt configuration used, while Figure 4-1(b) shows the previous weld configuration. Welding the actual head and skirt together was not practically possible due to cost constraints and since a larger than available test bench would be required. Therefore samples representing the two different head-to-skirt weld configurations were made using the dimensions of the above mentioned column as a base line. It is thought that it may show the difference in fatigue life between the two geometries and determine how accurately the numerical methods can predict the fatigue life.

It was thought that two plates welded at an angle will give a reasonable approximation of the head-to-skirt junction, even though the curvature of the skirt and head is not taken into account. For the specific column an angle of 20°, gives the best approximation of the curvature on the head as shown in Figure 4-1. However, it is not possible to weld the plates at this small angle due to access constraints. Therefore an angle of 30° was chosen as this gives sufficient access for welding of the plates and still provides a reasonable approximation of the angle between the head and skirt for the column chosen.

The second concern was which material to use. These columns are typically build from either SA 516 Gr 70, which is a carbon steel or SA 240 304L, which is a stainless steel. Stainless steels have a lower thermal conductivity than carbon steels, which causes more displacements during welding. As displacement is one of the aspects that were studied it was decided to build the samples from stainless steel.

Thirdly the thickness of the plate was chosen as 6 mm as according to Maddox (Maddox, 1991) thin sections produce the greatest displacement problem. Thicker welded samples also pose a problem since a stronger than anticipated test bench would be required.

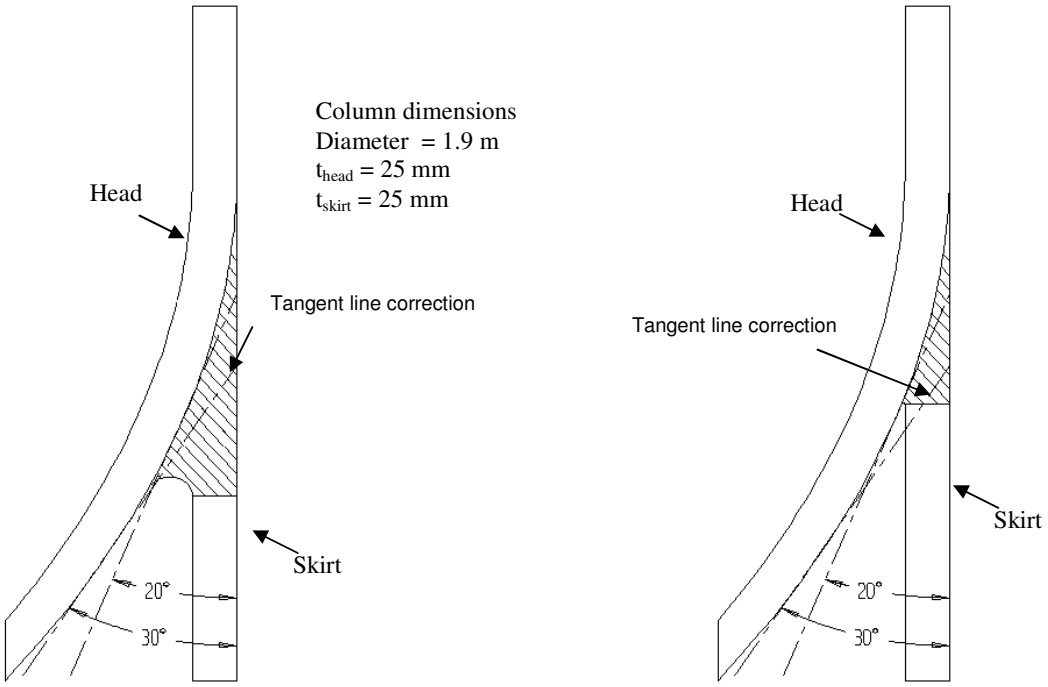

a) Modified weld geometry with weld build-up (Geometry 1)

b) Weld geometry without weld build-up (Geometry 2)

Figure 4-1: Schematic representation of the head-to-skirt weld for a specific column indicating two tangent lines to the head.

Figure 4-2 shows the configuration of the samples chosen to simulate the two different geometries of the head-to-skirt junctions presented in Figure 4-1.

1. Geometry 1 has a weld build-up with a 2 mm radius between the head-to-skirt junction and approximates the modified weld geometry on the Sasol Standard.
2. Geometry 2 has no weld build-up between the head-to-skirt junction. GTAW re-melting of the weld root is done by welding an autogenous GTAW weld pass between the head and the skirt. This was done as it is a proven technique to increase fatigue life on welding as the initial crack present at the weld root is eliminated (Maddox & Mantghi, 2004:1). This geometry approximates the old Sasol geometry, with GTAW re-melting added.

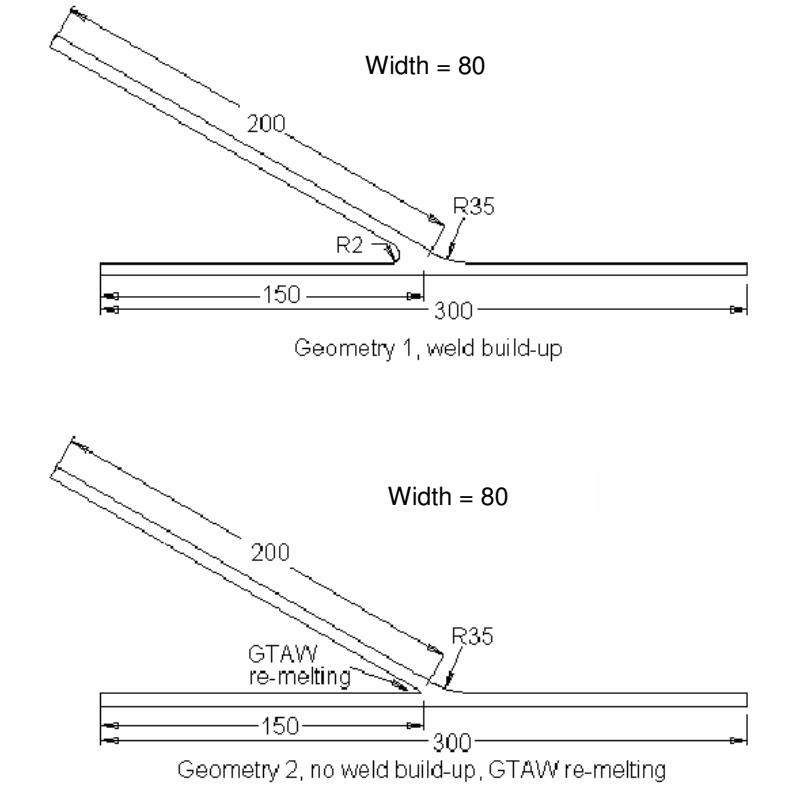

Figure 4-2: Schematic representation of the chosen weld geometries to test.

4.2 Manufacturing of fatigue samples

4.2.1 Number of samples

To draw up a weld S-N curve for these weld geometries, samples needed to be tested at various loads. However, this would require a great number of samples to be welded and tested, for which no budget and time was available. It was therefore decided to construct four samples of Geometry 1 and four samples of Geometry 2 and test these at the same fluctuating load condition provided by an actuator. This would give a limited amount of experimental data, but it is though that this approach could suffice to give a base for further fatigue predictions of the head-to-skirt weld and possibly illustrate the difference, if any, in the fatigue life of the two geometries as a first approximation.

4.2.2 Weld procedure

A typical weld sequence, for the head-to-skirt weld, used in industry, is shown in Figure 4-3 (Coetzee, 2005). A short section of the skirt, usually about 300 mm long is first welded to the head. This is done by doing weld build-up on the head, then attaching the short skirt section and welding the area between the head and skirt. The reason for only attaching a short piece of skirt is to gain access to weld between the

head and skirt. This weld between the head and skirt is then back-ground to give the minimum radius requested by the Sasol Standard drawing. Back-gouging from the outside of the skirt is now done to sound metal. The welding required on the outside of the head-to-skirt junction is now completed and lastly the weld is grinded smooth. Next, the required non-destructive testing of the weld is done, which include ultrasonic testing and magnetic particle testing. If no defects are detected during the non-destructive testing the lower skirt can be attached. If defects are detected this weld is repaired before attaching the lower skirt section.

Figure 4-4 and Table 4-1 show the weld sequence and processes used for the manufacturing of both test Geometries based on the WPS's used by industry to manufacture the head-to-skirt weld on tall columns. The weld sequence was kept as close as possible to that used in industry; however the following changes were required. A more detailed account of the WPS is presented in Appendix A.

Normally weld passes 1 and 3 to 8 are to be made by means of SAW (Submerged Arc Welding), however SAW equipment was not available at the university for use. It was therefore decided to use the GMAW (Gas Metal Arc Welding) process for these weld passes. As the process of welding is not taken into account when classifying the welds into a fatigue class it is thought that this change would have a negligible effect on the fatigue prediction (Hobbacher, 2004:47).

The welding of the samples was done at the University of Pretoria. An automated work bench available in their laboratory was used. The automated work bench was used as it is easier to control the weld speed, power input and feed rate of filler with an automated process than by hand. For both geometries the same processes and sequence was followed for weld passes 1 to 8.

For weld pass 1, the GMAW wire guide and the gas shield was clamped onto the work bench and then set to run at 10mm/s. This speed was obtained by measuring the time it took the GMAW tip to run 100mm. The bottom plate of samples were sequentially clamped onto a weld jig by using clamping plates 1 and 2 (See Section 4.2.3 for details of clamps and weld jig). A run-on and run-off plate was positioned next to the area to be welded. A shielding gas of 98% Argon and 2% Helium was used. The flow of the shielding gas was set to 12 liter per minute, but varied between about 8 liter per minute and 14 liter per minute during the welding. Stainless Steel filler wire (A 307) of diameter 1.2 mm was used and fed to the sample at a rate of 74 mm/s using an automatic wire feeder. The potential difference and current during welding was measured using a wire clamp, for all weld passes. For weld pass 1 the value set obtained were 200 Amps and 29 Volts. Weld pass 1 was allowed to cool for 30 seconds, before the plate was removed from the weld jig.

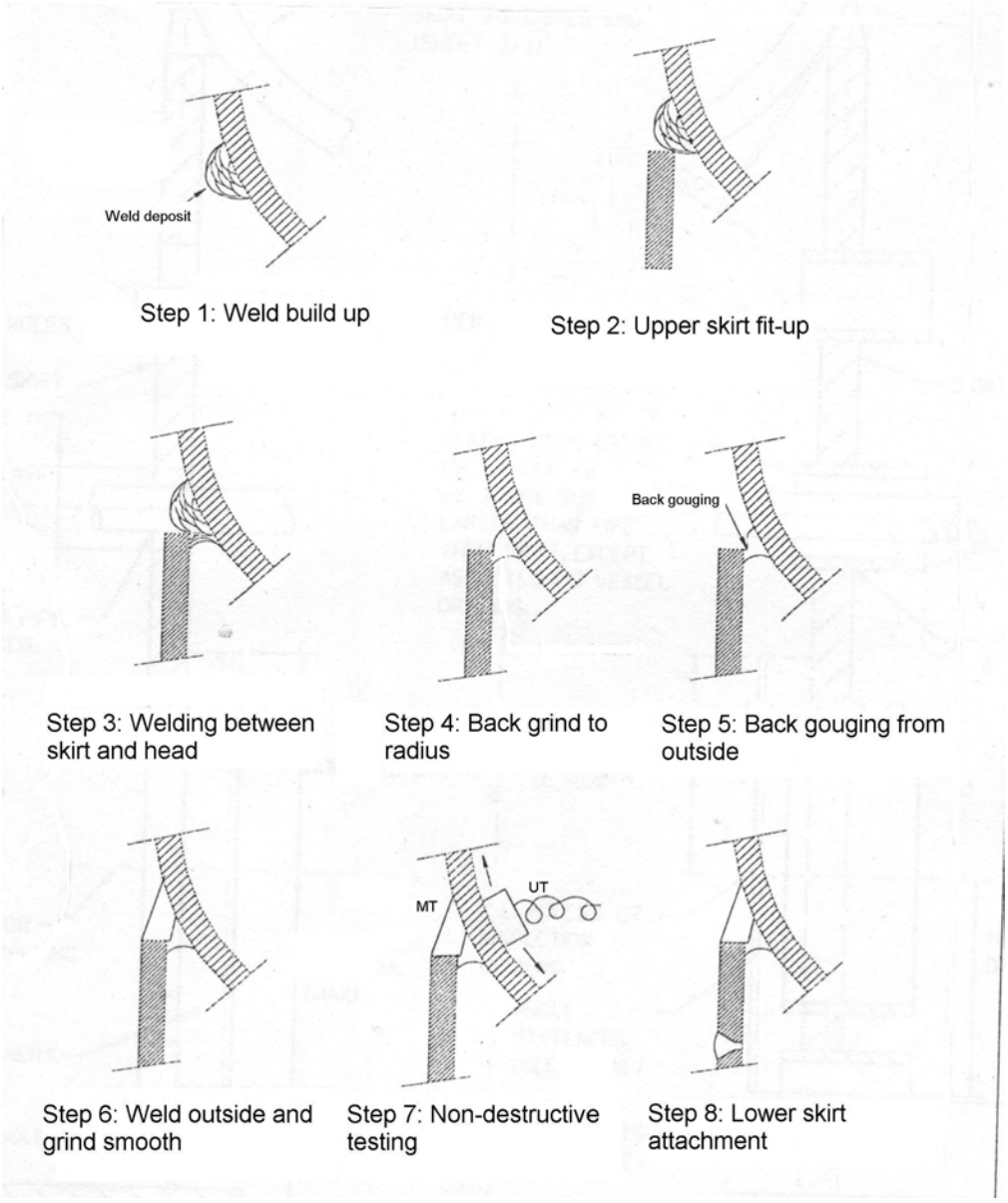

Figure 4-3: A typical weld sequence used in industry to manufacture head-to-skirt junctions in vertical pressure vessels supported by a skirt.

The welded bottom plate was then left to cool to room temperature. The leg displacement after welding was measured as described in Section 4.2.7 before machining the top 1 mm from the deposited weld metal. The welded bottom plate was then again clamped in place on the weld jig together with the top plate, which has an edge prep of 45° machined on it.

For weld pass 2 an autogenous weld pass was done to weld the top plate to the bottom weld. Again the gas nozzle with the tungsten electrode was clamped into the welding bench and set to weld at a travel speed of 10 mm/s. The same shielding gas as for weld pass 1 was used with a direct current electrode negative set up. The current difference measured during welding of weld pass 2 was 228 Amps at a potential difference of 15 Volts. The weld was allowed to cool for 30 seconds before it was removed from

the weld jig and allowed to cool to room temperature. The leg displacements of the top and bottom plate were measured again.

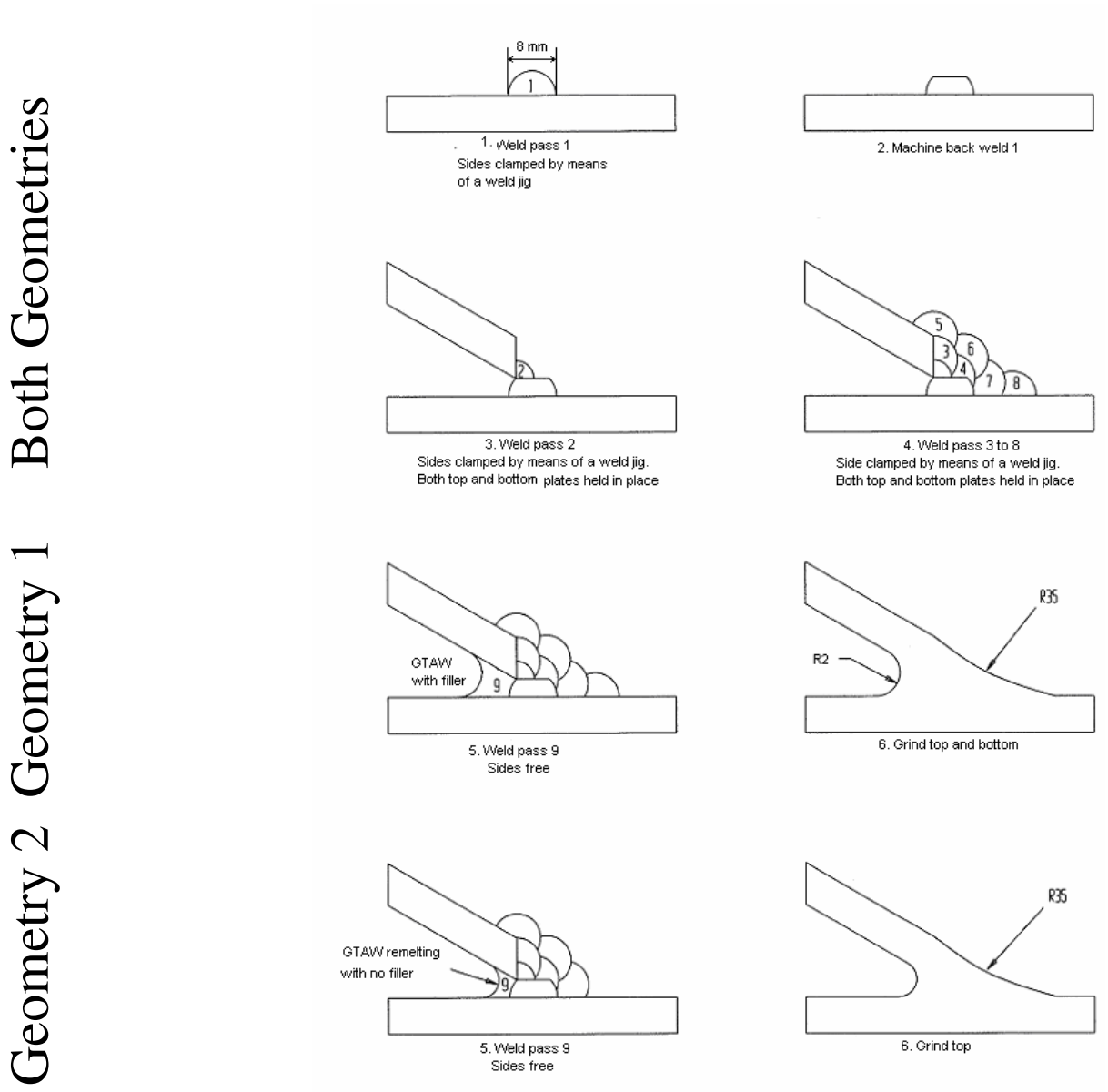

Notes:

1. Run-on and run-off plates used for passes 1-8
2. Weld pass 1, 2 and 8 allowed cooling for 30 seconds before the welded samples was removed from the jig
3. Weld pass 3-7 allowed cooling for 120 seconds before next weld pass was to be made

Figure 4-4: Welding sequence followed to construct the fatigue test samples. Weld jig used is shown in Figure 4-5.

For weld pass 3 to 8 plates were again clamped into position on the weld jig. It was made by means of the GMAW process, with the same set-up as used for weld pass 1. However the current was reduced to 90 Amps and the potential difference to 18 Volts. The wire feed rate was increased to 95.25 mm/s. Between each weld pass the weld was allowed to cool for 120 seconds before the next weld pass was made. After weld pass 8 was completed the samples were allowed to cool for 30 seconds before it was removed from

the weld jig and cooled to room temperature. The resulting leg displacement as a result of welding was measured for the top and bottom plate.

Weld pass 9 for Geometry 1 was carried out by means of the GTAW process. For this weld pass the sample was not clamped into the weld jig as it did not provide sufficient access. Weld pass 9 was welded free hand by the work shop manager. The same shielding gas was used. A 2mm filler wire of 316 Stainless Steel was used. The travel speed was measured at approximately 5.8 mm/s, with the potential difference equal to 22 Volts and a current equal to 150 Amps. The sample was allowed to cool to room temperature before back grinding the top to approximately 35 mm radius and the inside angle to a 2 mm radius. The top radius was measured by using a plastic circle with a 35 mm. The final leg displacements for both plates of the samples of Geometry 1 were then measured.

Table 4-1: Process and Process variables used for each weld pass geometry

	Geometry 1	Geometry 2
Weld pass 1		
Process	GMAW	GMAW
Amps	200	200
Volts	29	29
Travel speed (mm/s)	10	10
Filler	307 SS	307 SS
Weld pass 2		
Process	GTAW	GTAW
Amps	228	228
Volts	15	15
Travel speed (mm/s)	10	10
Filler	Autogenous	Autogenous
Weld pass 3-8		
Process	GMAW	GMAW
Amps	90	90
Volts	18	18
Travel speed (mm/s)	10	10
Filler	307 SS	307 SS
Weld pass 9		
Process	GTAW	GTAW
Amps	150	150
Volts	22	22
Travel speed (mm/s)	5.8	5.8
Filler	316SS	Autogenous

Weld pass 9 for Geometry 2 was welded by means of the GTAW process. Again the sample was not clamped into the weld jig as it did not provide sufficient access. Weld pass 9 was welded free hand by the work shop manager. The same shielding gas was used. *No filler metal* was added as only GTAW re-melting was required. The travel speed was measured at approximately 5.8 mm/s, with the potential

difference equal to 22 Volts and the current equal to 150 Amps. The sample was allowed to cool to room temperature before back grinding the top to approximately 35 mm radius. The top radius was measured by using a plastic circle with 35 mm. The final leg displacements for both plates of the samples of Geometry 2 were then measured.

4.2.3 Weld Jig

Figure 4-5 shows the weld jig used to manufacture the samples. A detailed drawing is presented in Appendix C. As discussed, welds 1 to 8 as shown in Figure 4-4 were made with the samples clamped onto the weld jig. For weld 9 no weld jig was used as the weld jig did not allow access to the root of the weld between the two plates. The weld jig was constructed from mild steel.

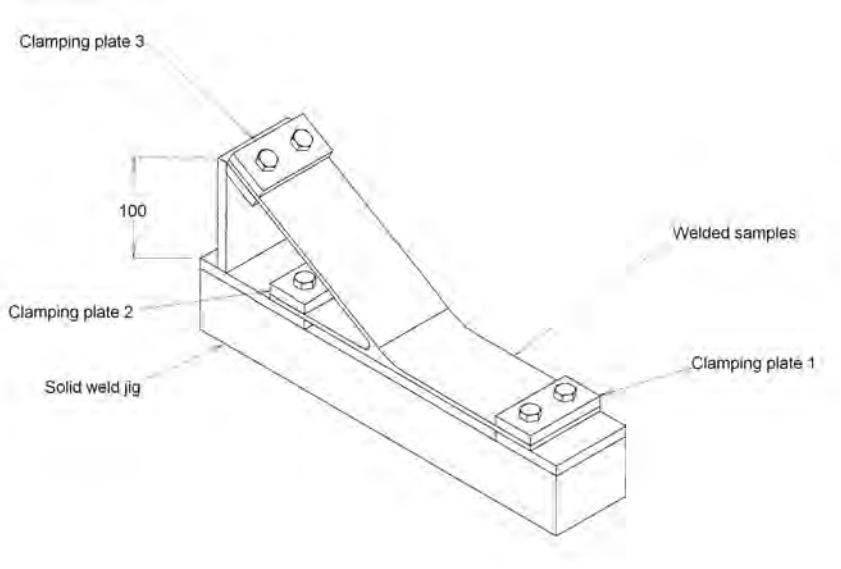

Figure 4-5: The weld jig used to manufacture welded samples.

4.2.4 Non-destructive testing of the welds

The non-destructive testing done on the completed welded samples included only dye penetrant testing. This ensured that there were no surface cracks or defects in the samples. Embedded defects in the samples could however still be present, but due to the weld geometry and sample thickness it was not possible to detect these.

4.2.5 Leg displacement due to welding

The displacements due to welding of samples were measured after the first, second, eighth and final weld as the weld sequence presented in Figure 4-4 progressed. All displacements were measured by placing points 1 and 2 on a flat work bench (reference plane). Leg positions were measured at reference positions 3 and 4 from which the displacement (Δl) due to welding was determined (Figure 4-6). The distances to points 3 and 4 were measured by placing a ruler 90 degrees to the workbench. Only upward displacements were measured and are captured in Table 4-2 (Final displacements) and Appendix B.2 (Intermediate displacements). For Geometry 1 an average upwards displacement of 18.5 mm was obtained at point 3 and an average upwards displacement of 22 mm was obtained at point 4. For Geometry 2 an average upwards displacement of 16 mm was obtained at point 3 and an average upwards displacement of 29 mm was obtained at point 4.

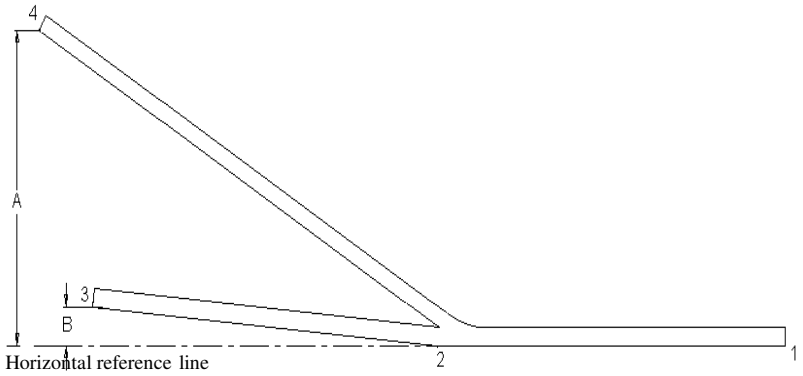

Figure 4-6: Schematic of a welded sample showing the positions (3 and 4) from which displacements A and B were respectively measured to determine sample leg displacements.

Table 4-2: Leg displacements (3 and 4) of the final welded samples for Geometry 1 and Geometry 2 after back grinding. All dimensions are given in mm.

	Distance A[(1)] l_d	Displacement $\Delta l = l_d - l_o$	Distance B[(1)] l_d	Displacement $\Delta l = l_d - l_o$
Geometry 1				
Sample 1	122	22	18	18
Sample 2	122	22	19	19
Sample 3	123	23	18	18
Sample 4	122	22	19	19
Average	122	22	18.5	18.5
Geometry 2				
Sample 1	129	29	16	16
Sample 2	129	29	16	16
Sample 3	128	28	17	17
Sample 4	130	30	16	16
Average	129	29	16	16

Notes:
(1) Starting distance before welding (l_0) 0 mm, from horizontal reference line.
(2) Starting distance before welding (l_0) 100 mm, from horizontal reference line.

5 Fatigue testing

5.1 Fatigue test rig

A photo of the test rig used to carry out fatigue testing of the welded samples is shown in Figure 5-1. Figure 5-2 shows a schematic representation of the fatigue setup that was used. Figure 5-3 shows the components used to connect the samples to the actuator.

These components consisted of a stable base built from mild steel onto which the samples were clamped. Two clamping plates connected the test piece to the base. A connector rod assembly and a clamping plate connected the free end of the test piece to the actuator rod end, (type GAR 15DO, Appendix D), to ensure that only up and down motions were transferred to the test piece. A computer with the necessary software was used to generate the input signal to the hydraulic actuator and to analyze digital signals from the analog to digital converter as received from strain gauge 1, glued on the active leg of the welded sample.

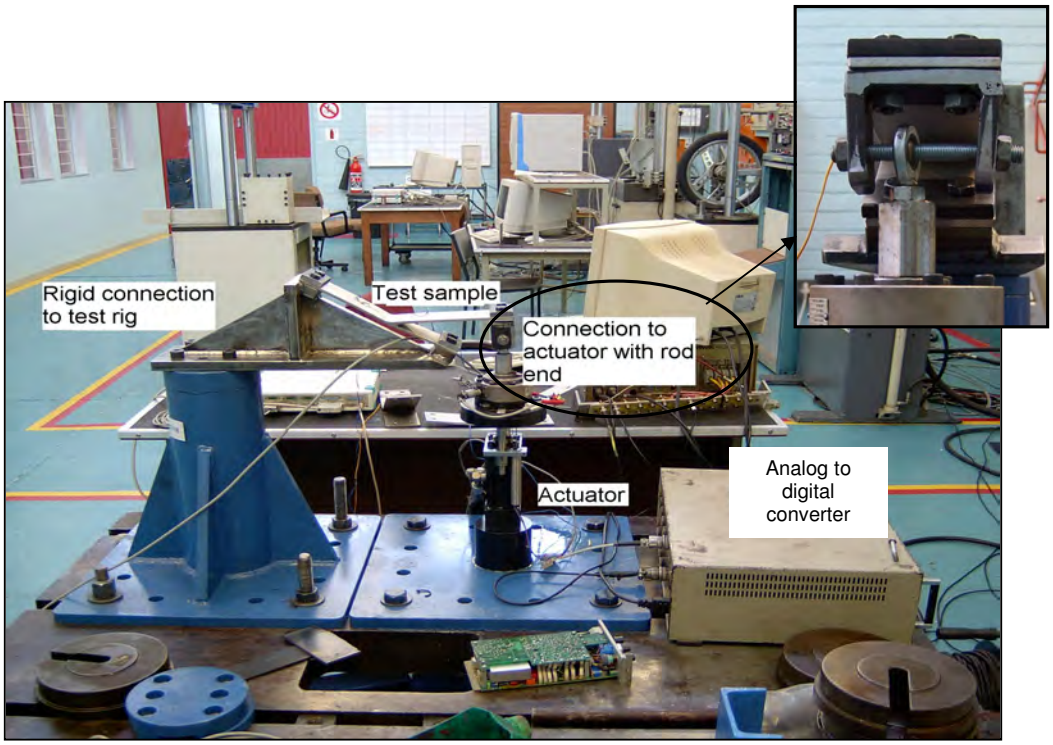

Figure 5-1 Photo of the test rig used for the fatigue testing of the welded samples

Detail drawings of the mild steel base and of both connector rod assemblies used for the fatigue tests are shown in Appendix C.

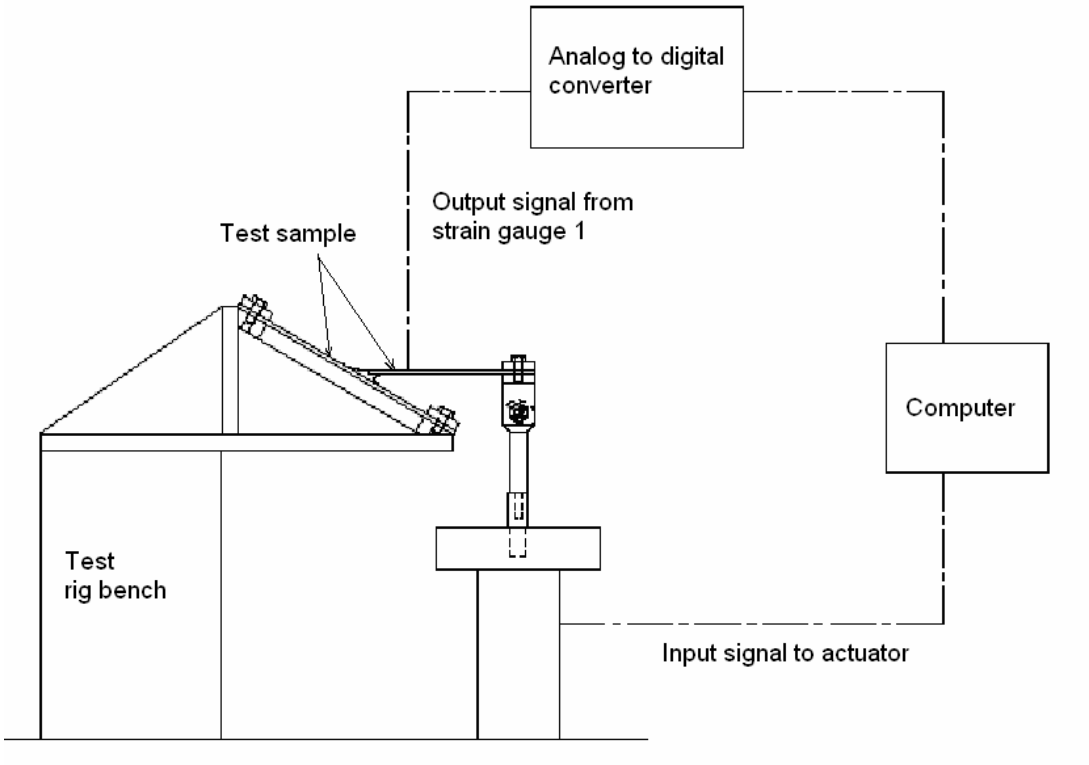

Figure 5-2: Schematic representation of fatigue setup used

5.2 Fatigue test set-up and input signal

Two linear strain gauges that were glued to the active and static leg of the test sample were used to measure surface deformation (effective strain). Linear strain gauges were chosen as strain in one direction only was expected. The strain gauges used was supplied by HMB. Both strain gauges had a measuring grid of 3 mm with a 120 Ω resistance. All HBM strain gauges are self compensating for temperature by matching the strain gauge to the thermal expansion of the material to be tested. The type of strain gauge used is of type 1-LY15-3/120. Generic information on the strain gauges used is presented in Appendix E.

The strain gauge positions are shown in Figure 5-4. The strain gauges were bonded to the samples by means of Z70 adhesive. The strain gauges were supplied with solder ends and the gauge leads was soldered to the strain gauges. The leads were then bonded to the sample with epoxy to limit stresses on the strain gauge to lead connections. Both strain gauges were connected in a quarter bridge configuration. The strain gauges were calibrated by applying a shunt resistor over the active strain gauge before use to determine which voltage output would represent a corresponding strain. An overview of the procedure carried out for strain gauge calibration in presented in Appendix B.1.

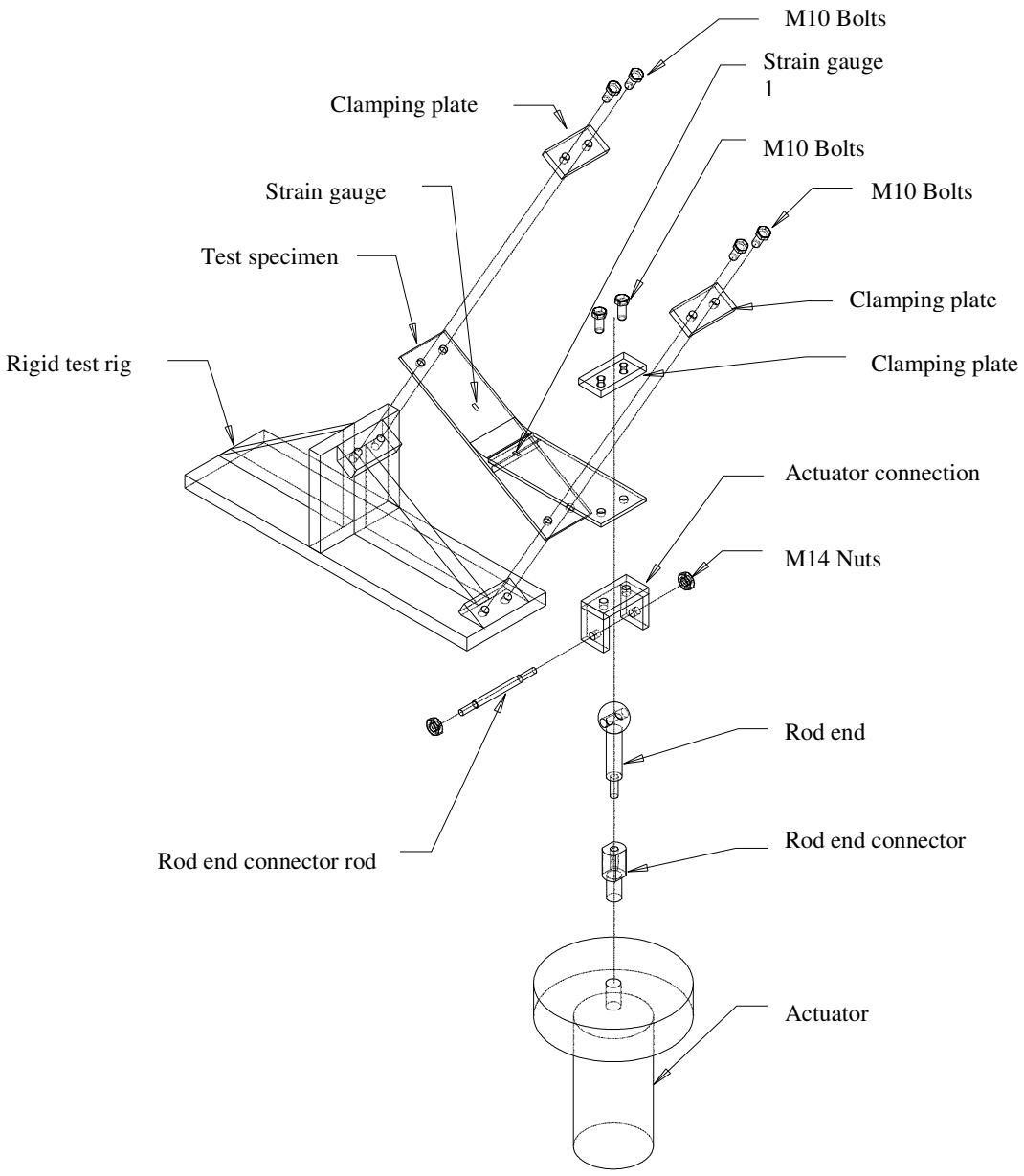

Figure 5-3 Detail of the base and connectors used to connect the samples to the actuator.

The fatigue tests were done in displacement control mode and not load control mode as there was no load cell available for load control purposes. A completely reversible sine wave, with a displacement amplitude of 4.8 mm, was created on the computer as the driving signal to the hydraulic actuator. The output strain from the strain gauge was then recorded.

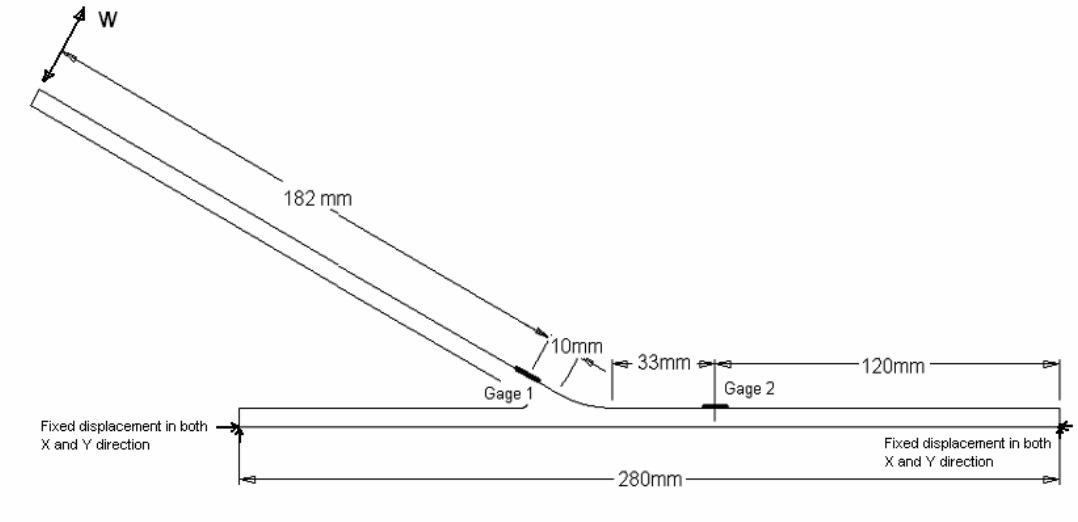

Figure 5-4: Illustration of how the samples were constrained during testing and how the load was applied. Strain gauge positions are also shown.

To verify the leg displacement of the test sample the actuator was manipulated manually until the same maximum and minimum values was found on strain gauge 1. The actual upwards and downwards displacement obtained during testing was then measured by means of a caliper. The strain on strain gauge 2 was recorded at this maximum displacement amplitude. This was the only time that the strain value on strain gauge 2 was recorded, as the analog to digital converter could only read one signal continuously back to the computer during testing.

The maximum frequency at which the tests could be conducted was found to be 10Hz. At this frequency the actuator could follow the input signal and did not create any high frequency signals. Due to the low frequency at which the tests could be conducted the testing of one sample took about 15 hours.

5.3 Process followed during fatigue testing

For the fatigue tests the following procedure was followed. A completely reversible sine wave with a displacement amplitude of 4.8 mm was sent to the hydraulic actuator from the computer for 30 seconds at the frequency specified in Table 5-1. The computer recorded the change in volts from strain gauge 1, glued to the active leg of the test sample, at 0.01 second intervals. These readings were then all converted to positive values and were all summed together to get a base line change in volt value for a sample without any defects.

After each 30 second block the summed change in volt value obtained from the strain gauge 1 was compared to the base line value. When a 20% deviation from the base line was obtained the test was terminated. This deviation was found to correspond to a visual crack that had formed on the inside of the

sample at the top plate in the heat affected zone of the weld. The tests were therefore terminated once the maximum strain in the samples had decreased by 20%. Appendix F.1 gives a flow diagram of the steps followed.

5.4 Fatigue Test Results

The results of the fatigue tests run are presented in Table 5-1. While testing Sample 2 of Geometry 1 the actuator malfunctioned and broke the test sample, therefore the results of Sample 2 as shown in Table 5-1, should be discarded. After the actuator was repaired, the maximum frequency at which the tests could be carried out was found to be only 8 Hz. The final two samples of each geometry were then tested at 8 Hz.

Table 5-1: Results of the fatigue tests

	Geometry 1				Geometry 2			
Test nr	Test frequency	Number of Cycles till crack	Volts amplitude on strain gauge 1 in mV/V	Volts amplitude on strain gauge 2 in mV/V	Test frequency	Number of Cycles till crack	Volts amplitude on strain gauge 1	Volts amplitude on strain gauge 2
1	10 Hz	537 300	0.431	0.117	10 Hz	294 000	0.430	0.114
2	10 Hz	449 100	0.450	0.115	10 Hz	199 200	0.450	0.118
3	8 Hz	597 360	0.440	0.117	8 Hz	247 680	0.438	0.117
4	8 Hz	477 120	0.433	0.114	8 Hz	203 040	0.440	0.115
Average		537 260 (Test 2 excluded)	0.439	0.116		235 980	0.439	0.116

The average maximum amplitude readings obtained on the strain gauges during testing were 0.439 mV/V on strain gauge 1 and 0.116 mV/V on strain gauge 2. These maximum values where obtained when the maximum displacement of 4.8 mm was applied to the sample in upwards and downwards directions. The difference in strain gauge readings for the various samples can be attributed to the strain gauges positions differing slightly on the samples.

By using the strain gauge calibration as shown in Appendix B.1, where there was found that a change of 1 mV/V on the output signal correspond to a change in strain of 1990.06 με, therefore the mV/V readings on strain gauge 1 correspond to 874 μm/m strain and on strain gauge 2 to 231 μm/m strain.

6 Life Predictions from Simple Fatigue Prediction methods

In this section simple, single axial fatigue prediction methods are employed in an effort to predict the life of the tested samples. As discussed in Section 2.4.2.5 the Nominal-Stress-Approach and the Hot-Spot-Stress-Approach does not consider the physical weld geometry and is therefore unable to distinguish between the two different weld geometries tested. However, from discussions with Sasol (Coetzee, 2005) it was thought that it may be useful to still predict the fatigue life by means of the Nominal-Stress-Approach, which uses a weld SN curve, due to the fact that most codes are based on a similar approach. This will therefore give an indication of what predicted life can be expected when using SN curve type approaches.

It was therefore decided to employ the Nominal-Stress-Approach, the Effective-Notch-Stress-Approach and the Stress-Life-Approach, as discussed in Chapter 2, to predict the fatigue life of the tested samples.

The same approach will be applied for all the prediction methods. Firstly, the finite element model used to obtain the life prediction is verified against the data from the strain gauges. Then the stresses at the weld toe obtained from this model are used to make the life prediction. Lastly, the predicted life is verified against the life actually obtained in order to see how accurate the specific approach predicted the fatigue life and if the approaches distinguished between the two different geometries.

A convergence of at least 95% was obtained for all finite element models, but due to historic reasons this can not be presented here.

6.1 Nominal-Stress-Approach

6.1.1 Stress determination

For the Nominal-Stress-Approach only the nominal stress present in the sample should be used for the determination of the fatigue life. For simple geometries it is possible to use the beam bending equations from Shigley (2001:1180) to determine this stress.

For the geometry being investigated it would be possible to assume that the sample is constrained as shown in Figure 6-1. This then reduces the problem to that of a cantilever beam with a clamped end.

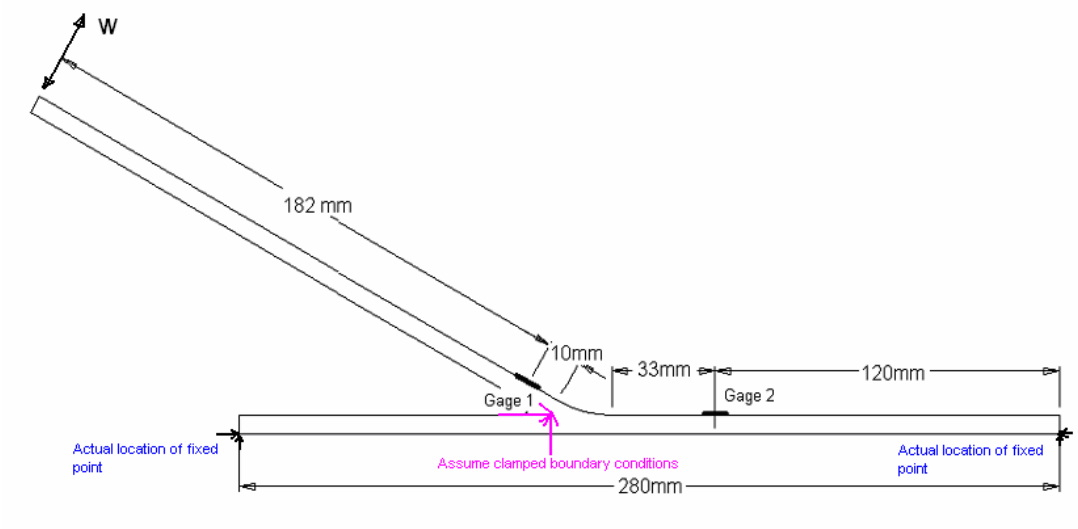

Figure 6-1: Illustration of how the sample geometry can be simplified to enable the use of simple beam theories to predict the stresses in the samples.

The maximum stress is expected to occur in the sample when the maximum displacement amplitude of 4.8 mm is applied to the sample. This displacement corresponds to a load (W) of 557N. However before the maximum expected stress at the weld root can be determined the stress at the strain gauge position should be determined to determine if the stresses calculated by the above assumption correspond to that measured.

The stress at strain gauge 1 was found to be 209 MPa, by using the beam bending equations. However during testing a strain of 874 µm/m (Section 5-4) was measured on strain gauge 1. The Youngs modulus of elasticity for SA 304 Stainless Steel is 190 GPa, therefore the measured strain correspond to a stress of 166 MPa. This is considerably smaller than that calculated by the above assumption of a clamped cantilever beam in bending.

The most likely cause for this is that the bottom plate deformed during the fatigue tests as the samples was only constrained at the ends of the bottom plate as shown in Figure 5-4. Considering the sample to be clamped at the weld as shown in Figure 6-1 create to high a constraint on the sample and therefore to high a stress is predicted. This theory is also supported by the stress of 43.9MPa measured at strain gauge 2, which suggest that some bending occurred in the bottom plate (As is verified with the finite element analysis in Section 6.1.2). Therefore a more rigorous approach through finite element analysis is required.

6.1.2 Finite element verification

For the Nominal-Stress-Approach a shell model is used as described by Hobbacher (2004:25). The shell model consists of 5550 Q8, shell elements and 17083 nodes. A linear elastic finite element model was

used with the following material properties for the SA 304 Stainless Steel: Youngs modulus of 190GPa and Poisson ratio of 0.3. The analysis was run in MD Nastran 2006r1.

The weld was modeled by adding shell elements (Figure 6-2), on each side of the weld. As the actual weld geometry can not be modeled by means of shell elements, the modeling procedure as described in Hobbacher (2004:25) allow for stiffening elements to be added to simulate the actual stiffness of the welded area. The added elements do not need to correspond to the weld size or weld geometry in anyway.

For this specific model various element sizes was added, but it was found that adding an element of 2.5 mm on either side of the weld gave enough stiffness to the model to give a correlation of less than 10% between the experimentally obtained stresses at the strain gauge positions and the finite element predicted stresses.

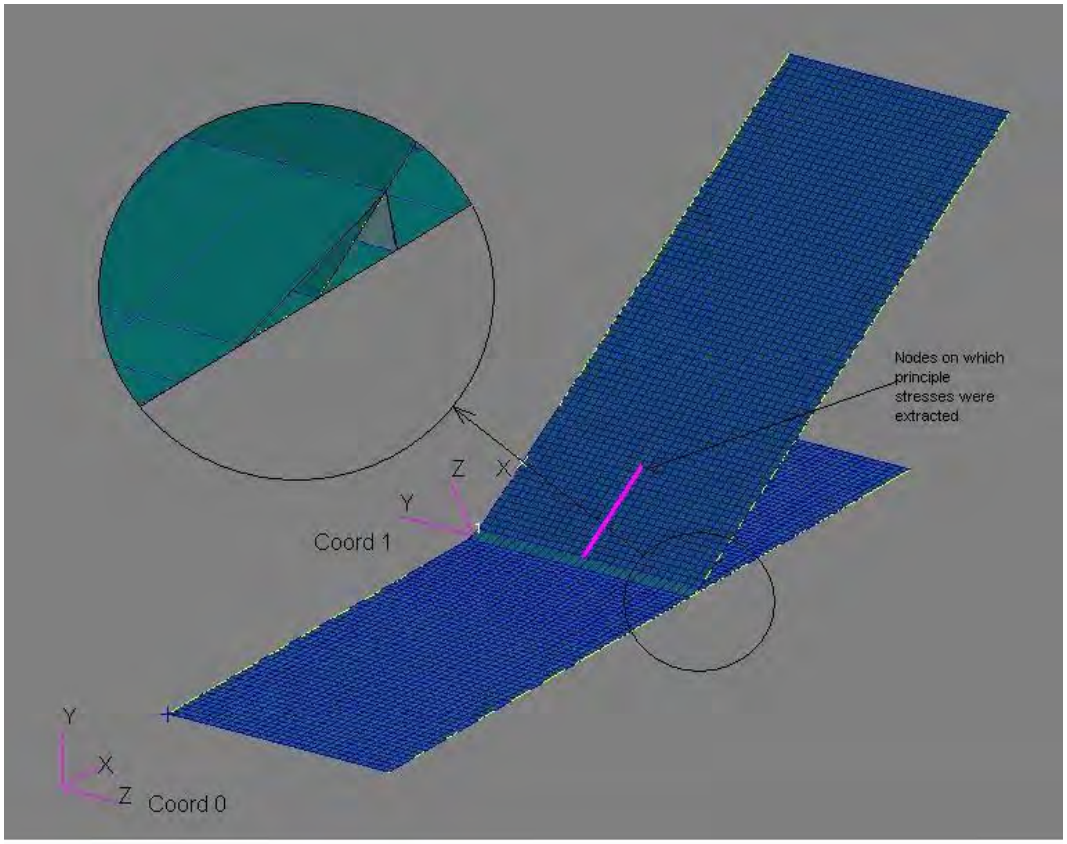

Figure 6-2: Finite element model used for the prediction of stresses in the Nominal-Stress-Approach

Figure 6-2 shows the model used in the finite element analysis. All dimensions and boundary conditions used represent the real test conditions as near as possible. The model consists of two plates, the top one with a length of 192 mm and the bottom one with a length of 280 mm. Both plates have a thickness of 6 mm and a width of 80 mm. For the bottom plate, fixed boundary conditions were used on both sides to

simulate the clamped boundary condition during testing. A displacement of 4.8 mm was applied to the top plate in the z-direction, of coordinate axis 1, to simulate the maximum displacement, as described in Section 5-2.

From the model the stresses at the strain gauge positions were extracted. These are compared to the average experimentally measured strain gauge values from Section 5-4 in Table 6.1. The strain gauge measurements are converted to stress by multiplying the strains by 190 GPa, the same elasticity modulus as for the finite element model. From this it is evident that the results obtained have an error estimate of about 9% on strain gauge 1. Thus it can be concluded that this model could be used to provide valid nominal stress values at the weld.

Table 6-1: Comparison of stresses at strain gauge position

Strain gauge 1			Strain gauge 2		
FEM	Test	Error	FEM	Test	Error
181 MPa	166 MPa	9%	43.6 MPa	43.9 MPa	0.68%

Figure 6-3 shows the displacements obtained from the finite element analysis. This clearly demonstrates that the samples bent through during the fatigue tests and therefore the beam bending equations did not give accurate results.

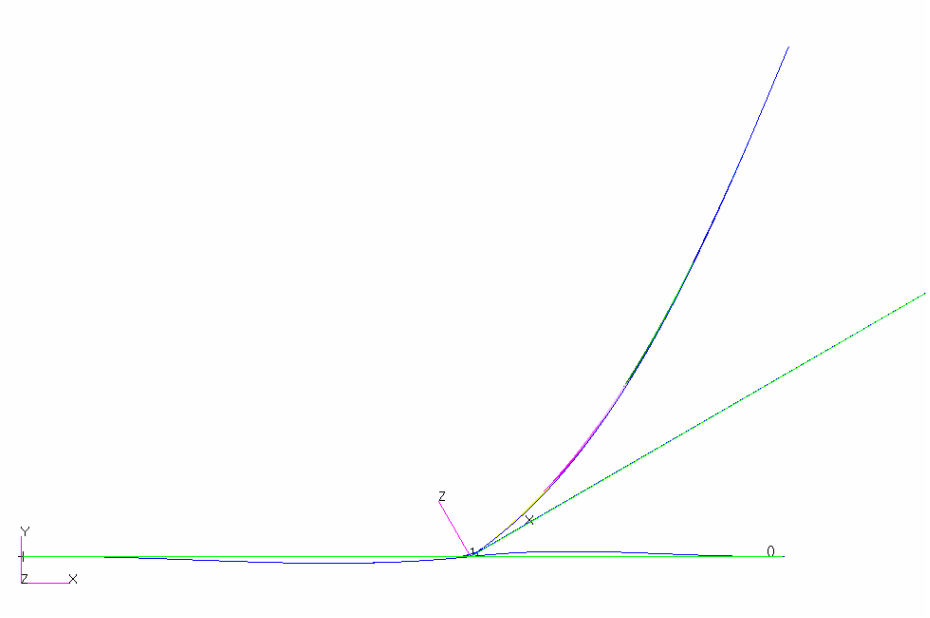

Figure 6-3: Displacements obtained when the maximum 4.8 mm displacement is applied on the sample in the upward direction. A scale of 30% is used.

6.1.3 Nominal stress at weld

The maximum principle stress at the weld was extracted from the finite element model. This was obtained by extracting the maximum principle stress values on Coord 0, in the top plane as shown in Figure 6-22. The maximum principle stress at the weld toe was found to be 190 MPa and used as such in the fatigue predictions to follow.

6.1.4 Fatigue life

The S-N curves from Hobbacher (2004:60) were used to determine the expected life of the samples. The weld was classed as a full penetration T-joint (detail 411) corresponding to a FAT class of 80.

For Geometry 1 an improvement factor of 1.3 on stress range was taken into account as the samples were background at the weld toe from which fatigue failure occurred (Hobbacher, 2004:86). This led to a fatigue life prediction of 41 000 cycles for Geometry 1 as based on detailed calculations presented in Appendix B.3.

For Geometry 2 no back grinding at the weld toe was done, only GTAW re-melting. Therefore the improvement factor for grinding could not be taken into account. The improvement factor for GTAW re-melting can only be taken into account if the plate thickness is more than 10 mm and therefore was not used either (Hobbacher, 2004:87). The fatigue life predicted for Geometry 2 was found to be 18 662 cycles as based on detailed calculations presented in Appendix B.3.

6.2 Effective-Notch-Stress-Approach

This section focuses on the fatigue life predicted for the welded samples by means of the Effective-Notch-Stress-Approach.

6.2.1 Finite element verification

For the local notch stress approach the finite element verification proved more of a challenge than for the Nominal-Stress-Approach. This was due to the fact that the specific geometry of the welded joint needed to be analyzed. This posed the first problem: does one analyze the deformed or un-deformed welded sample?

In reality the load or displacement will be applied to the deformed sample after welding, but during the design phase the deformed shape was not always known. Thus the first step was to find out how the stresses in the finite element model of the un-deformed geometry compared to that of the deformed geometry.

All the finite element models were chosen to be plane strain models. A linear elastic finite element analysis was run on Msc. Nastran for all four geometries. All models used Q8 elements, with the following material properties: Youngs modulus of 190 GPa and Poisson ratio of 0.3.

Model 1, (Figure 6-4a) Geometry 1 without taking displacements into account, consisted of two flat plates. The bottom plate has a length of 280 mm and the top plate has a length of 192 mm. Both of the plates were modeled as 6 mm thick and 80 mm wide. The top plate was connected at an angle of 30 degrees to the bottom plate, see Figure 6-1. The finite element model consisted of 10039 nodes and 3122 elements. The bottom plate was constraint in all directions on the ends and a displacement of 4.8 mm was applied to the top plate in the Y direction of coord 1.

Model 2, (Figure 6-4b) Geometry 1 taking displacements into account, consisted of two flat plates. The bottom plate has a length of 280 mm and the top plate has with a length of 192 mm. Both of the plates were modeled as 6 mm thick and 80 mm wide. For the model the displacements obtained during welding, as given in Table 4-2, was taken into account. The bottom plate was modeled with a displacement of 18.5 mm upwards and the top plate was modeled with an additional displacement of 22 mm upwards from the 30 degree plane. The finite element model consisted of 9495 nodes and 2938 elements. The bottom plate was constraint in all directions on the ends and a displacement of 4.8 mm was applied to the top plate in the Y direction of coord 1.

Model 3, (Figure 6-4c) Geometry 2 without taking displacements into account, consisted of two flat plates. The bottom plate has a length of 280 mm and the top plate has a length of 192 mm. Both of the plates were modeled as 6 mm thick and 80 mm wide. The top plate was connected at an angle of 30 degrees to the bottom plate, see Figure 6-1. The finite element model consisted of 13109 nodes and 4132 elements. The bottom plate was constraint in all directions on the ends and a displacement of 4.8 mm was applied to the top plate in the Y direction of coord 1.

Model 4, (Figure 6-4d) Geometry 2 taking displacements into account consisted, of two flat plates. The bottom plate has a length of 280 mm and the top plate has with a length of 192 mm. Both of the plates were modeled as 6 mm thick and 80 mm wide. For the model the displacements obtained during welding,

as given in Table 4-2, was taken into account. The bottom plate was modeled with a displacement of 16 mm upwards and the top plate was modeled with an additional displacement of 29 mm upwards from the 30 degree plane. The finite element model consisted of 13801 nodes and 4352 elements. The bottom plate was constraint in all directions on the ends and a displacement of 4.8 mm was applied to the top plate in the Y direction of coord 1.

From all the finite element models the stresses at the strain gauge positions were extracted and are presented in Table 6-2. The measured strain gauge readings were converted to stress by using the same Youngs modulus as for the finite element model, 190 GPa. The predicted stresses and the average stress readings at the strain gauge positions were compared. For strain gauge position 1 a maximum error estimate of 7.2% was found when the deformed shape of Geometry 1 was analyzed. For strain gauge 2 a maximum error estimate of about 22.8 % was found when the deformed shape of Geometry 1 was analyzed. This should still be in the acceptable range and therefore these models can be used to determine the maximum stress at the weld toe for use in the Effective-Notch-Stress-Approach.

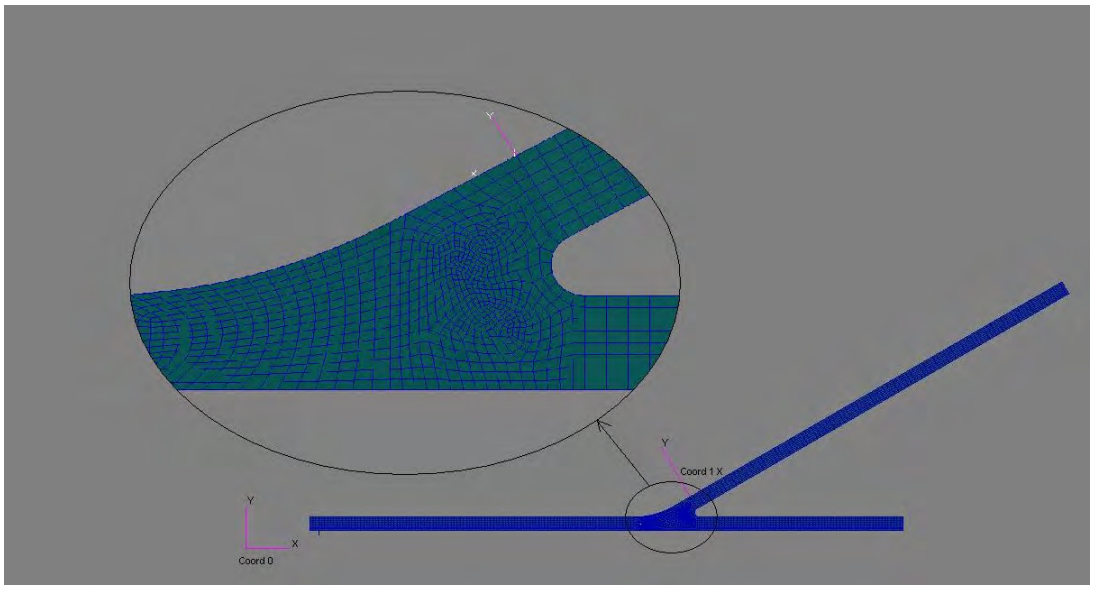

Figure 6-4a) Finite element model of Geometry 1 without taking the displacements that occurred during welding into account.

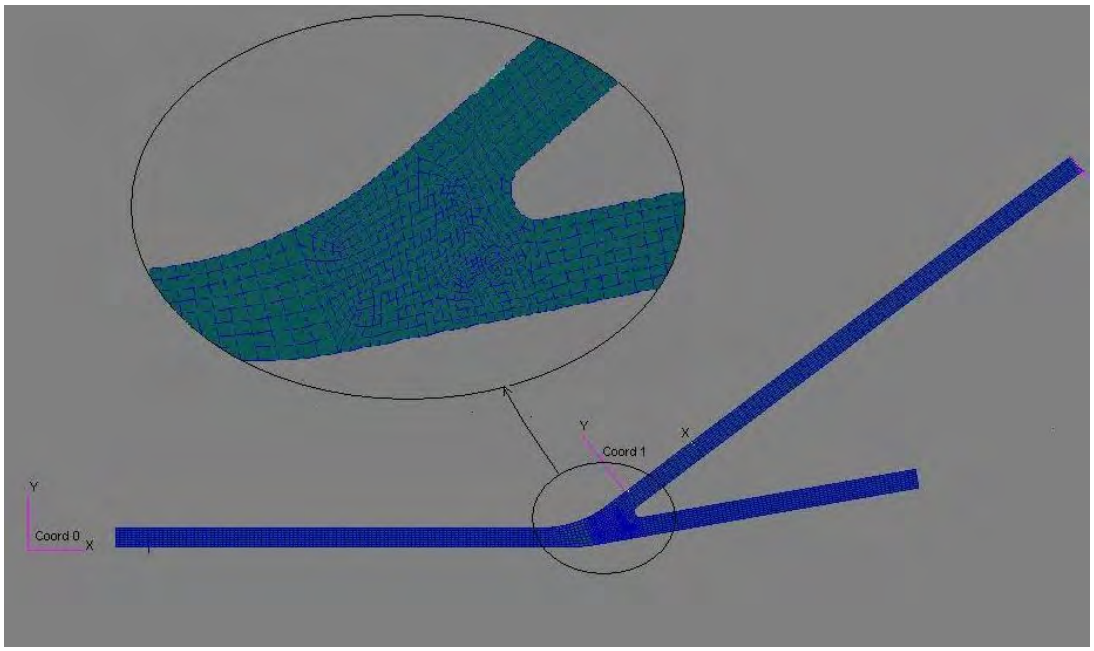

Figure 6-4b) Finite element model of Geometry 1 taking the displacements that occurred during welding into account.

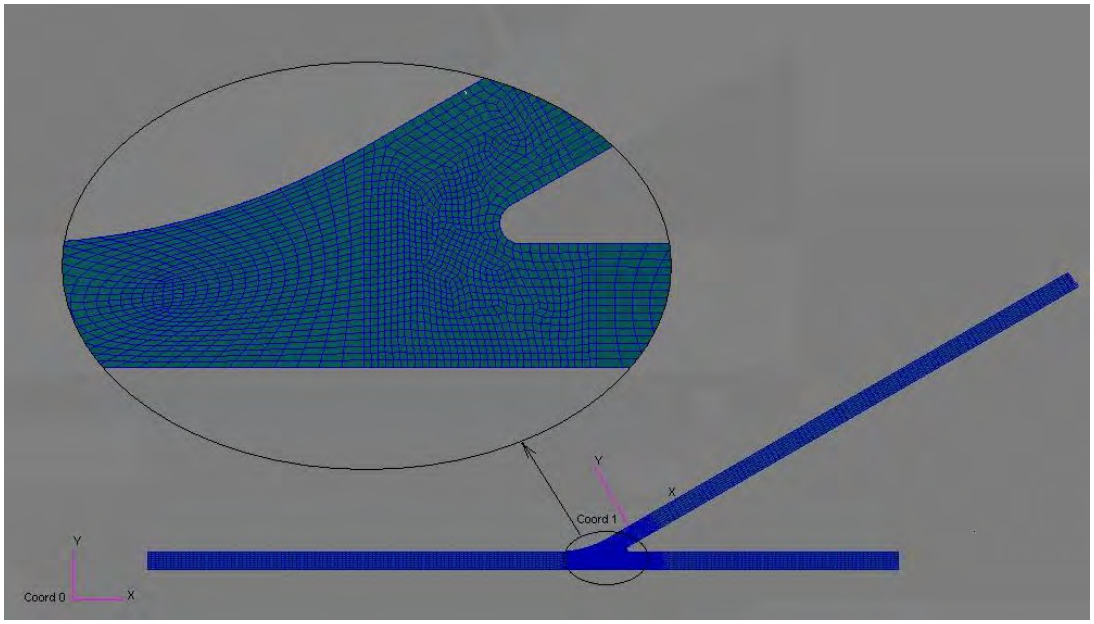

Figure 6-4c) Finite element model of Geometry 2 without taking the displacements that occurred during welding into account.

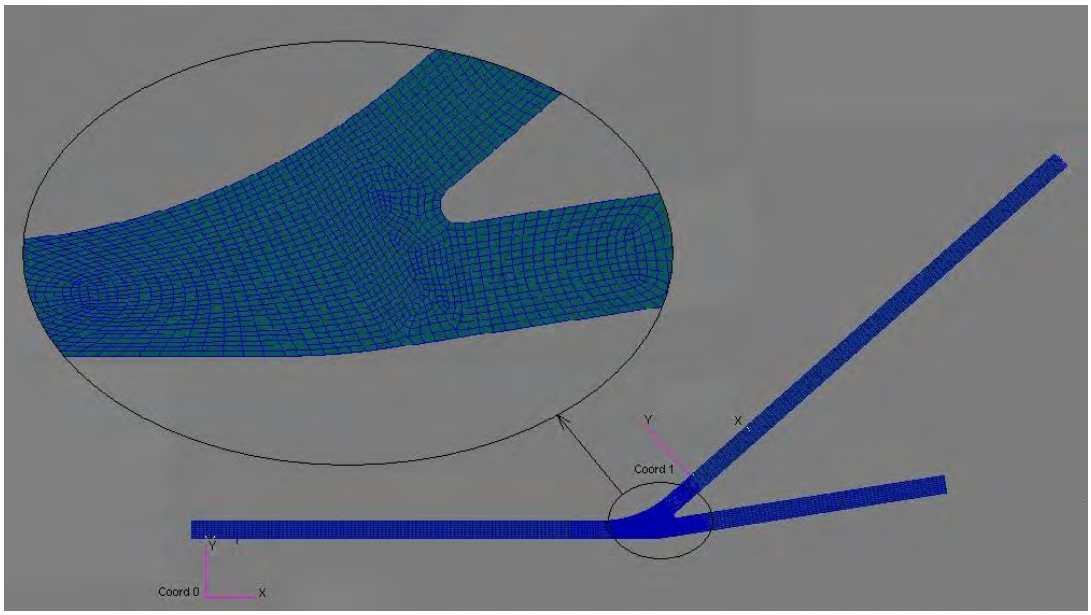

Figure 6-4d) Finite element model of Geometry 2 taking the displacements that occurred during welding into account.

Figure 6-4: Plane strain models used for Effective-Notch-Stress-Approach

Table 6-2: Comparison of stresses at strain gauge position

Description	Strain gauge 1			Strain gauge 2		
	FEM	Test	Error	FEM	Test	Error
Geometry 1, Un-deformed	177 MPa	166 MPa	6.6%	34.6 MPa	43.9 MPa	21.2%
Geometry 1, Deformed	178 MPa	166 MPa	7.2%	33.9 MPa	43.9 MPa	22.8%
Geometry 2, Un-deformed	174 MPa	166 MPa	4.8%	37.4 MPa	43.9 MPa	14.8%
Geometry 2, Deformed	176 MPa	166 MPa	6.0%	41.3 MPa	43.9 MPa	5.9%

6.2.2 Fatigue life

As described by Hobbacher (2004:80) a universal fatigue curve for all welded structures is used to determine the fatigue life of the samples. For this approach the maximum principle stress at the expected crack position is used. This is read off from the linear elastic finite element models that were verified in the above section.

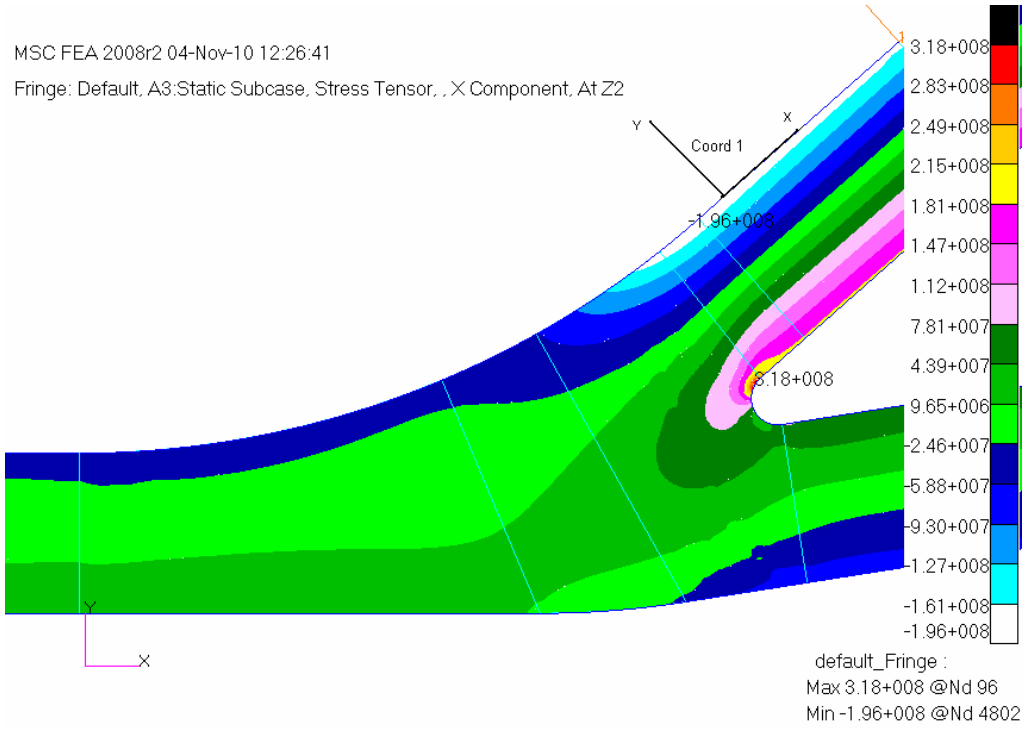

Figure 6-5: Fringe stress distribution plot of the normal stress in the x-direction of Coord 1, obtained from the finite element analysis results for the un-deformed configuration of Geometry 1.

Figure 6-4 shows the stress results obtained from the finite element model of Geometry 1 in the un-deformed shape. This clearly shows that the highest stress value is obtained at the position where the cracks initiated during testing.

Table 6-3 lists the maximum stresses obtained and fatigue lives predicted by each of the models, as based on detailed calculations presented in Appendix B.4. It is evident from this table that the finite element model of the un-deformed shape of Geometry 1, predicts the stress for the deformed shape of Geometry 1 within 1 MPa. The finite element model of the un-deformed shape for Geometry 2 over predicts the stress by about 6%. Furthermore the error in life prediction between the deformed shape and the un-deformed shape for Geometry 1 is 1.1% and for Geometry 2 is 15%. One can therefore conclude that the un-deformed shapes can be used to predict the fatigue life.

Table 6-3: Maximum stress and fatigue life predicted by means of the Effective-Notch-Stress-Approach

Description	Geometry 1			Geometry 2		
	Un-deformed Shape [1]	Deformed Shape [2]	% Difference	Un-deformed Shape [1]	Deformed Shape [2]	% Difference
Maximum Stress	280 MPa	281 MPa	0.4%	351 MPa	332 MPa	6%
Number of predicted cycles till failure	129 721	128 342	1.1%	65 852	77 817	15.38%

Notes:
[1] Displacements due to welding not taken into account when modeling the weld in the finite element analysis.
[2] Displacements due to welding taken into account when modeling the weld in the finite element analysis.

6.3 Stress Life Relationship

Both the Nominal-Stress-Approach and the Effective-Notch-Stress-Approach gives conservative estimates of the expected fatigue life of the sample. Therefore the principles as described in Shigley (2001:367) were used to determine if a better approximation of the fatigue life of the samples can be obtained.

Using an ultimate stress of 505MPa and the endurance limit modifying factors, the fatigue life of the samples can be predicted.
The following modification factors were used:

- Surface factor, k_a, equal to 0.925, by using the factors for a ground sample from Shigley (2001:375),
- Size factor, k_b, equal to 0.914, the effective diameter calculated for the samples was substituted into the bending equation from Shigley (2001:376),
- Load factor, k_c, equal to 1, as the samples is in bending (Shigley 2001:377)
- Temperature factor, k_d, chosen as 1.01. The temperature was not measured during testing, but an increase in temperature of the test sample could be felt. A temperature of 50°C was therefore chosen (Shigley 2001:379).
- Miscellaneous effects factor, k_e.

No specific guidelines are given in Shigley (2001:381) on what the miscellaneous effect factor should be. For this specific analysis it was chosen as 1.

By using the stresses obtained in Section 6.1.2 and Section 6.2.2 the static stress concentration factor was determined. For Geometry 1 this was found to be 1.27 regardless of whether deformations due to welding were taken into account or not. For Geometry 2 the stress concentration was found to be 1.4 if deformation is not taken into account and 1.35 when deformation is taken into account. However the fatigue stress concentration factor needs to be calculated to determine the stress that should be used to predict the expected fatigue life of the samples. Equation 2 from Section 2.4.2.4 was used with r equal to 2 for Geometry 1 and r equal to 1 for Geometry 2. For both geometries a transverse hole configuration for Heywood's parameter ($\sqrt{a}$) was chosen. (Shigley, 2001:383)

The fatigue stress concentration factor (k_f) was now determined as 1.27 for Geometry 1, whether deformation due to welding is taken into account or not. For Geometry 2 the fatigue stress concentration

factor was found to be 1.4 if deformations are not taken into account and 1.35 if deformations are taken into account.

Table 6-4 Number of cycles until failure predicted by means of the stress life relationship. The fatigue stress concentrations factors and stresses used to predict the fatigue life of the samples is also given.

	Geometry 1		Geometry 2	
	Un-deformed shape[1]	Deformed shape[2]	Un-deformed shape[1]	Deformed shape[2]
δ_{Max}[3] in MPa	281	280	351	332
δ_a[4] in MPa	190	190	190	190
K_t	1.47	1.47	1.40	1.75
r in mm	2	2	1	1
$\sqrt{a}$ [5]	0.345	0.345	0.345	0.345
K_f	1.27	1.27	1.40	1.35
$\delta_a \times K_f$ in MPa	243	242	267	256
Predicted cycles until failure	320 628	329 474	117 264	178 333

Notes:
[1] Displacements due to welding not taken into account when modeling the weld in the finite element analysis.
[2] Displacements due to welding taken into account when modeling the weld in the finite element analysis.
[3] Maximum principle stresses obtained from the finite element analyses in Section 6.2.1, Table 6-2.
[4] Nominal stress obtained from the finite element analysis in Section 6.1.2.
[5] Heywood's parameter for a transverse hole.

Using the fatigue stress concentrations and the nominal stress from Section 6.1.2 the expected fatigue lives was determined; this is indicted in Table 6-4. For Geometry 1 this was found to be 320 638 cycles until failure if deformation due to welding is not taken into account. This increases to 329 474 cycles until failure when the displacements are considered. For Geometry 2 the predicted number of cycles until failure was found to be 117 264 if deformation is not taken into account and this increased to 178 333 cycles until failure if the deformations was considered.

7 Discussion

7.1 General

The fatigue tests as described in Section 5 were done on two different geometries using four samples of each weld geometry. In was reported in Section 5.4 that Geometry 1, produced with weld build-up, lasted almost twice as long as Geometry 2, the sample finished with GTAW re-melting only. This clearly demonstrates that the fatigue life can be improved by doing weld build-up and regrinding to an increased inner contact radius.

Table 7-1 compares the experimental results for each weld geometry with the results obtained from the Nominal-Stress-Approach calculations presented in Section 6.1.3. This shows that the Nominal-Stress-Approach is overly conservative in the prediction of the fatigue life of the samples. The samples on average lasted 13 times longer than predicted by the Nominal-Stress-Approach.

Table 7-1 Comparison of the experimentally obtained fatigue life and the fatigue life predicted by means of the Nominal-Stress-Approach

	Geometry 1			Geometry 2		
	Experimentally obtained life[(1)]	Cycle Life predicted by the Nominal-Stress-Approach[(2)]	Error Factor [(3)]	Experimentally obtained life[(1)]	Cycle Life predicted by the Nominal-Stress-Approach[(2)]	Error Factor [(3)]
Test 1	537 300	41 000	13.1	294 000	18 662	15.8
Test 2	Not usable			199 200	18 662	10.7
Test 3	597 360	41 000	14.6	247 680	18 662	13.3
Test 4	477 120	41 000	11.6	203 040	18 662	10.9
Average	537 260	41 000	13.1	235 980	18 662	12.6

Notes:
[(1)] Number of cycles obtained by means of testing.
[(2)] Number of cycles obtained by means of the Nominal-Stress-Approach
[(3)] Amount of times that the predicted life is smaller than the experimentally obtained life

As discussed in Section 2.4.2.5 there was expected that the Nominal-Stress-Approach will not distinguish between the two weld geometries, as the local weld geometry is not taken into account when calculating the stress for use in the fatigue life predictions. However the difference in predicted fatigue life as shown in Table 7-1 can be attributed to the fatigue improvement factor for back grinding that was taken into account on Geometry 1. For GTAW re-melting the same improvement factor can be taken into account if the welded sections are more than 10 mm thick, however as the samples only had a thickness of 6mm, this improvement factor could not be taken into account, and therefore the difference in fatigue life predicted.

Table 7-2 compares the experimental results for each geometry with the results obtained from the Effective-Notch-Stress-Approach calculations presented in Section 6.2.2. On average the samples of Geometry 1 lasted 4 times longer than predicted by the effective notch stress and those of Geometry 2 lasted 3.5 times longer when considering the un-deformed sample and 3 times longer when considering the deformed sample.

Table 7-2 Comparison of the experimentally obtained fatigue life and the fatigue life predicted by means of the Effective-Notch-Stress-Approach

Geometry 1 Effective notch stress					
	Experimentally obtained life[1]	Cycle Life predicted by the Effective-Notch-Stress-Approach (Displacements taken into account)[2]	Error Factor [3]	Cycle Life predicted by the Effective-Notch-Stress-Approach (Displacements not taken into account)[2]	Error Factor [3]
Test 1	537 300	129 722	4.0	128 342	4.2
Test 2	Not usable				
Test 3	597 360	129 722	4.6	128 342	4.7
Test 4	477 120	129 722	3.7	128 342	3.7
Average	537 260	129 722	4.1	128 342	4.2
Geometry 2 Effective notch stress					
	Experimentally obtained life[1]	Cycle Life predicted by the Effective-Notch-Stress-Approach (Displacements not taken into account)[2]	Error Factor [3]	Cycle Life predicted by the Effective-Notch-Stress-Approach (Displacements taken into account)[2]	Error Factor [3]
Test 1	294 000	65 852	4.5	77 817	3.8
Test 2	199 200	65 852	3.0	77 817	2.6
Test 3	247 680	65 852	3.8	77 817	3.2
Test 4	203 040	65 852	3.1	77 817	2.6
Average	235 980	65 852	3.6	77 817	3.0

Notes:
[1] Number of cycles obtained by means of testing.
[2] Number of cycles obtained by means of the Effective-Notch-Stress-Approach
[3] Amount of times that the predicted life is smaller than the experimentally obtained life

Furthermore, the results from the Effective-Notch-Stress-Approach indicate that this approach did distinguish between the two weld geometries. Although this approach did not provide the fatigue life obtained experimentally it correctly predicted the trend of failure with Geometry 1 failing later than Geometry 2.

Both the Nominal-Stress and Effective-Notch-Stress-Approaches gives overly conservative estimates for the fatigue life of the samples. There can be a few reasons for the error in life prediction.

Firstly the SN-curves, for both the Nominal-Stress-Approach and the Effective-Notch-Stress-Approach, created for the weld geometries have a safety factor incorporated into them. This safety factor according

to Hobbacher (2004:43) allows for at least a 95% probability of survival. However the values of the standard deviations required too reduce the probability of survival to 50% for each weld geometry is not given and therefore this safety factor could not be removed.

Secondly, the nearest default weld configuration for the Nominal-Stress-Approach calculation according to Hobbacher (2004:60) is a full penetration fillet weld which does not fully correspond to the weld configuration of the head-to-skirt weld. This was however the closes weld configuration that could be chosen, but could have led to an overly conservative estimate of the fatigue life.

Lastly, as discussed in Hobbacher (2004:86) and Maddox and Manteghi (2006:1) crack like discontinuities exist at the toes of welds. The presence of these discontinuities mean that normally fatigue in welded structures may occur more rapidly than in metals without welds as no time is spend in crack initiation as the crack is already present. However for both the weld geometries these initial cracks were removed, in Geometry 1 by grinding the weld toe and in Geometry 2 by doing GTAW re-melting. As the Nominal-Stress-Approach and the Effective-Notch-Stress-Approach would account for these crack like flaws the predicted fatigue life can be expected to be lower than the experimentally obtained values.

Table 7-3 Comparison of the experimentally obtained fatigue life and the fatigue life predicted by means of the Stress-Life-Approach

Geometry 1 Stress-Life-Approach					
	Experimentally obtained life[1]	Cycle Life predicted by the Stress-Life-Approach (Displacements not taken into account)[2]	Error Factor [3]	Cycle Life predicted by the Stress-Life-Approach (Displacements taken into account)[2]	Error Factor [3]
Test 1	537 300	320 638	1.68	329 474	1.63
Test 2	Not usable				
Test 3	597 360	320 638	1.86	329 474	1.81
Test 4	477 120	320 638	1.49	329 474	1.45
Average	537 260	320 638	1.68	329 474	1.63
Geometry 2 Stress-Life-Approach					
	Experimentally obtained life[1]	Cycle Life predicted by the Stress-Life-Approach (Displacements not taken into account)[2]	Error Factor Difference [3]	Cycle Life predicted by the Stress-Life-Approach (Displacements taken into account)[2]	Error Factor [3]
Test 1	294 000	117 264	2.51	178 333	1.65
Test 2	199 200	117 264	1.70	178 333	1.12
Test 3	247 680	117 264	2.11	178 333	1.39
Test 4	203 040	117 264	1.73	178 333	1.14
Average	235 980	117 264	2.01	178 333	1.32

Notes:
[1] Number of cycles obtained by means of testing.
[2] Number of cycles obtained by means of the Stress-Life-Approach
[3] Amount of times that the predicted life is smaller than the experimentally obtained life

As both fatigue approaches based on the work of Hobbacher (2004) gave overly conservative estimates of the fatigue life, it was decided to use the first principles Stress-Life-Approach as presented in Section 6.3. Table 7-3 compares the predicted fatigue life from Section 6.3 with the experimentally obtained fatigue life of each weld category.

With the Stress-Life-Approach it was found that the predicted fatigue life for Geometry 1, compared to the average experimentally obtained life is out with a factor of 1.6. For Geometry 2 the fatigue life calculation is out with a factor of 2 if the displacements due to welding are not taken into account. If the displacements due to welding are taken into account in the calculations the fatigue life predicted was out a factor of only 1.3.

The experimentally obtained fatigue life for Geometry 1 has a variation of 20% between the maximum and the minimum obtained fatigue life, while Geometry 2 has a 32 % variation. From this experimental variation it can be deducted that the fatigue of welded samples is not an exact science, variations in results is expected. The experimentally obtained fatigue life can therefore not be predicted exactly.

7.2 Conclusion

The aim of this study was to determine whether the new weld geometry as proposed in the modified Sasol Standard for tall columns was truly required by determining to what extent the head-to-skirt weld geometry influenced the fatigue life of the weld and what commonly used fatigue prediction methods could be used to good effect to predict this fatigue life.

To determine this, two samples geometries were used, Geometry 1 approximating the modified Sasol weld geometry and Geometry 2 having only GTAW re-melting done on the root. Fatigue tests were carried out on the samples and it was found that the samples with weld build-up (Geometry 1) lasted twice as long as the samples with only GTAW re-melting (Geometry 2).

The fatigue life of the samples was predicted by means of the Nominal-Stress-Approach, the Effective-Notch-Stress-Approach and the Stress-Life-Approach. The Nominal-Stress-Approach gave very conservative fatigue life predictions. The samples tested lasted on average 13 times longer than predicted by the Nominal-Stress-Approach.

The Effective-Notch-Stress-Approach gave a less conservative estimate of fatigue life. It however still predicted that the weld samples for Geometry 1 will last 4 times longer and for Geometry 2 that the welds

will last 3.6 times longer, if displacements are not considered in the calculations. By taking displacements into account a slightly more accurate result for Geometry 2 could be obtained.

The Stress-Life-Approach gave the most accurate results in predicting the fatigue life of the welds. The fatigue life was only underestimated by a factor of 1.6 for Geometry 1 and by a factor of 2 for Geometry 2 when the displacement obtained during welding is not taken into account. For Geometry 2 this factor improve to 1.3 is the displacement due to welding is taken into account.

It can therefore be concluded that the fatigue life are likely increase if weld build-up with regrinding is carried out as required by the new Sasol Standard (4001E, 2008), and that GTAW re-melting does not give the same extent of improvement. Both the Effective-Notch-Stress-Approach and the Stress-Life-Approach can distinguish between the different weld geometries with regards to fatigue life, but the Stress-Life-Approach yields a more accurate prediction of the fatigue life. If displacements due to welding can be measured it should be taken into account as more accurate stresses at the welds can be obtained resulting in more accurate life predictions. If displacements are not know the fatigue life can still be calculated as a more conservative estimate of the fatigue life is expected.

Bibliography

Cheng X., Fisher J.W., Prask H.J., Gnaupel-Herold T. Yen B.T. & Roy S. 2003. Residual stress modification by post-weld treatment and its beneficial effect on fatigue strength of welded structures. *International Journal of Fatigue*. 25:1259-1269.

Coetzee, C. 2005. Personal communication. Secunda. (Principle Mechanical Engineer at Sasol Technology, Secunda)

Dong, P. & Hong, J.K. 2002. Analysis of IIW X/XV RSDP Phase I Round-Robin Residual Stress Results. *Welding in the World*. 46:24-31.

Du Toit, M. 2004. Class notes - Advanced Course in Welding Metallurgy. (Presented at the University of Pretoria Department of Material Science and Metallurgical Engineering)

Hobbacher, A. 2004. Recommendations for fatigue design of welded joints and components. IIW document XIII-1965-03/XV-1127-03. 146 p.

Lindgren, L.E. 2001. Finite Element Modelling and Simulation of Welding Part 1: Increased Complexity. *Journal of Thermal Stresses*. 24:141-192.

Maddox S.J. 1991. Fatigue strength of welded structures. Cambridge university press: Abington.

Maddox, S.J & Manteghi, S. 2004. Methods for fatigue life improvement of welded joints in medium and high strength steels. IIW Documents No. XIII-2006-04. 79 p.

Murugan S., Rai S.K., Kumar P.V., Jayakumar T., Ray B. & Bose M.S.C. 2001. Temperature distribution and residual stresses due to multipass welding in type 304 stainless steel and low carbon steel weld pads. *International Journal of Pressure Vessel and Piping*. 78:307-317, February.

Niemi E. 1995. Stress determination for fatigue analysis of welded components. IIS/IIW-1221-93. Cambridge: Abington Publishing. 69 p.

Niemi, E.J. & Marquis, G.B. 2003. Structural hot spot stress method for fatigue analysis of welded components. Metal structures - Design, Fabrication, Economy. Rotterdam: Mill Press.

Radaj D. 1996. Review of fatigue strength assessment of non welded and welded structures based on local parameters. *International Journal of Fatigue*. 18:153-170.

Sasol Project Document. 2008. Vessel categorization list for MIBK II, rev. 4. 2p

Sasol Project Document. 2010. Vessel categorization list for EPU 5, rev. 3. 2p

Sasol Standard. 1988. STDD-4001E, Vertical Vessel Support Details - General skirt details, rev 0. 1 p.

Sasol Standard. 2008. STDD-4001E, Vertical Vessel Support Details - General skirt details, rev 5. 1 p.

Shigley, J.E. & Mischke C.R. 2001. Mechanical Engineering Design. 6th Ed. Singapore: McGraw Hill. 1248 p.

Department of Labor. South Africa 2008. Occupational Health and safety Act and Regulations, 85 of 1993 (Full version). Pretoria: Interpak Books.

Teng T.L., Fung C.H. & Chang P.H. 2002. Effect of weld geometry and residual stresses on fatigue in butt-welded structures. *International Journal of Pressure Vessel and Piping*. 79:467-482, May

The American Society of Mechanical Engineers. 2008. ASME VIII Division 1 Rules for construction of Pressure Vessels. 2007 ASME Boiler and Pressure Vessel Code 2008a Addenda. New York. 755p.

The American Society of Mechanical Engineers. 2008. ASME IX Qualification Standard for Welding and Brazing Procedures, Welders, Brazers and Welding and Brazing Operators. 2007 ASME Boiler and Pressure Vessel Code 2008a Addenda. New York. 340p.

Turnmill Proquip. 2006. FEA report, Replacement Alcohol Water Splitter Column 237VL-102 R1. 1p

Van Tonder, F. 2004. Experimental strain measurement using strain gauges. (Class notes for course presented at the University of Pretoria)

Appendix A: WPS for welded samples

WELDING PROCEDURE SPECIFICATION (WPS) FOR LIZE BRINK MASTERS

WPS 01

GENERAL

Code/Test Standard	: ASME IX 2007 add 08	Support PQR	: Not qualified

JOINTS (QW-402)

Joint design	: As per drawing 1
Backing	: With backing

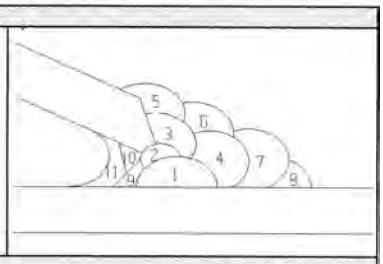

BASE METAL (QW 403)

Material 1	: SA 240 304 SS	Group no	: P No. 8 Gr No. 1
Material 2	: SA 240 304 SS	Group no	: P No. 8 Gr No. 1
Thickness base metal	: 6mm		
Maximum pass thickness	: 4mm		

FILLER METALS (QW 404)

Process	: GMAW	GTAW	GMAW	GTAW
Process type	: Automatic	Manual	Automatic	Manual
Filler Spec	: SFA 5.9	N/A	SFA 5.9	SFA 5.9
Filler Class Number	: AWS E307	N/A	AWS E307	AWS E316
Filler A Number	: A8	N/A	A8	A8
Filler F Number	: F6	N/A	F6	F6
Filler diameter	: 1.2 mm	N/A	1.2 mm	2mm
Filler metal product form	: bare metal	N/A	bare metal	bare metal
Wire feed rate	: 74 mm/s	N/A	95.25 mm/s	manual
Weld metal thickness				
Fillet	: See drawing	See drawing	See drawing	See drawing
Groove	: See drawing	See drawing	See drawing	See drawing

POSITION (QW 405)

Position of groove	: Flat 1G

PREHEAT (QW 406)

Preheat Temperature, :	0
Preheat Temperature, :	250

GAS (QW 408)

Type	: Mixture
% Comp	: 98% Ar - 2% He
Flow rate	: 8-14L/minute
Orifice	: 8-12mm ID
Trailing Gas	: None
Backing Gas	: None
Flow rate	: None

ELECTRICAL CHARACTERISTICS (QW 409)

		Filler metal		Current				
Weld Passes	Process	Classificatior	Diameter	Type and Polarity	Amps	Volts	Travel speed	Wire feed rate
1	GMAW	307 SS	1.2		200	29	10	74 mm/s
2	GTAW	Autogenou	Autogenous	DC -	228	15	10	none
3 to 8	GMAW	307 SS	1.2		90	18	10	95.25mm/s
9 to 11	GTAW	316 SS	2	DC -	150	22	5.8	manual

Tungsten electrode : 2% Thoriated

WELDING TECHNIQUE (QW 410)

Single/Multi pass	: Multipass	Oscillation	: N/A
Side welded	: One	Peening	: N/A
String/Weave Bead	: Stringer	Orific size	: 10mm
Filler Added	: Added	Method of cleaning	: Brushing
Solid/Tube wire	: Solid	Back gouging	: N/A
Tube-work distance	: 10mm	Single/Multi electrode	: Single
Electrode spacing	: N/A		

POST WELD HEAT TREATMENT (QW 407)

Heat rate	: N/A	Cool rate	: N/A
Hold temp	: N/A	Method	: N/A
Hold time	: N/A	Other	: No PWHT

Figure A.1: Welding Procedure Specification (WPS) used to weld geometry 1.

WELDING PROCEDURE SPECIFICATION (WPS) FOR LIZE BRINK MASTERS

WPS 01 modified

GENERAL

Code/Test Standard	: ASME IX 2007 add 08	Support PQR	: Not qualified

JOINTS (QW-402)

Joint design	: As per drawing 1
Backing	: With backing

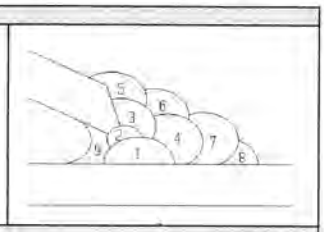

BASE METAL (QW 403)

Material 1	: SA 240 304 SS	Group no	: P No. 8 Gr No. 1
Material 2	: SA 240 304 SS	Group no	: P No. 8 Gr No. 1
Thickness base metal	: 6mm		
Maximum pass thickness	: 4mm		

FILLER METALS (QW 404)

Process	: GMAW	GTAW	GMAW	GTAW
Process type	: Automatic	Manual	Automatic	Manual
Filler Spec	: SFA 5.9	N/A	SFA 5.9	SFA 5.9
Filler Class Number	: AWS E307	N/A	AWS E307	AWS E316
Filler A Number	: A8	N/A	A8	A8
Filler F Number	: F6	N/A	F6	F6
Filler diameter	: 1.2 mm	N/A	1.2 mm	2mm
Filler metal product form	: bare metal	N/A	bare metal	bare metal
Wire feed rate	: 74 mm/s	N/A	95.25 mm/s	manual
Weld metal thickness				
Fillet	: See drawing	See drawing	See drawing	See drawing
Groove	: See drawing	See drawing	See drawing	See drawing

POSITION (QW 405)

Position of groove	: Flat 1G

PREHEAT (QW 406)

Preheat Temperature,	: 0
Preheat Temperature,	: 250

GAS (QW 408)

Type	: Mixture
% Comp	: 98% Ar - 2% He
Flow rate	: 8-14L/minute
Orifice	: 8-12mm ID
Trailing Gas	: None
Backing Gas	: None
Flow rate	: None

ELECTRICAL CHARACTERISTICS (QW 409)

		Filler metal		Type and	Current			
Weld Passes	Process	Classification	Diameter	Polarity	Amps	Volts	Travel speed	Wire feed rate
1	GMAW	307 SS	1.2		200	29	10	74 mm/s
2	GTAW	Autogenou	Autogenous	DC -	228	15	10	none
3 to 8	GMAW	307 SS	1.2		90	18	10	95.25mm/s
9	GTAW	316 SS	2	DC -	150	22	5.8	manual

Tungsten electrode : 2% Thoriated

WELDING TECHNIQUE (QW 410)

Single/Multi pass	: Multipass	Oscillation	: N/A
Side welded	: One	Peening	: N/A
String/Weave Bead	: Stringer	Orific size	: 10mm
Filler Added	: Added	Method of cleaning	: Brushing
Solid/Tube wire	: Solid	Back gouging	: N/A
Tube-work distance	: 10mm	Single/Multi electrode	: Single
Electrode spacing	: N/A		

POST WELD HEAT TREATMENT (QW 407)

Heat rate	: N/A	Cool rate	: N/A
Hold temp	: N/A	Method	: N/A
Hold time	: N/A	Other	: No PWHT

Figure A.2: Welding Procedure Specification (WPS) used to weld geometry 2.

WELDING PROCEDURE SPECIFICATION (WPS) FOR LIZE BRINK MASTERS

WPS 02

GENERAL

Code/Test Standard	: ASME IX 2007 add 08	Support PQR	: Not qualified

JOINTS (QW-402)

Joint design	: As per drawing 1
Backing	: With backing

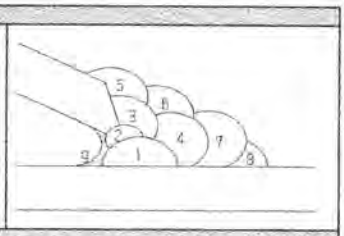

BASE METAL (QW 403)

Material 1	: SA 240 304 SS	Group no	: P No. 8 Gr No. 1
Material 2	: SA 240 304 SS	Group no	: P No. 8 Gr No. 1
Thickness base metal	: 6mm		
Maximum pass thickness	: 4mm		

FILLER METALS (QW 404)

Process	: GMAW	GTAW	GMAW
Process type	: Automatic	Manual	Automatic
Filler Spec	: SFA 5.9	N/A	SFA 5.9
Filler Class Number	: AWS E307	N/A	AWS E307
Filler A Number	: A8	N/A	A8
Filler F Number	: F6	N/A	F6
Filler diameter	: 1.2 mm	N/A	1.2 mm
Filler metal product form	: bare metal	N/A	bare metal
Wire feed rate	: 74 mm/s	N/A	95.25 mm/s
Weld metal thickness			
Fillet	: See drawing	See drawing	See drawing
Groove	: See drawing	See drawing	See drawing

POSITION (QW 405)

Position of groove	: Flat 1G

PREHEAT (QW 406)

Preheat Temperature, :	0
Preheat Temperature, :	250

GAS (QW 408)

Type	: Mixture
% Comp	: 98% Ar - 2% He
Flow rate	: 8-14L/minute
Orifice	: 8-12mm ID
Trailing Gas	: None
Backing Gas	: None
Flow rate	: None

ELECTRICAL CHARACTERISTICS (QW 408)

		Filler metal		Type and	Current			
Weld Passes	Process	Classificatior	Diameter	Polarity	Amps	Volts	Travel speed	Wire feed rate
1	GMAW	307 SS	1.2		200	29	10	74 mm/s
2	GTAW	Autogenou	Autogenous	DC -	228	15	10	none
3 to 8	GMAW	307 SS	1.2		90	18	10	95.25mm/s
9	GTAW	Autogenou	2	DC -	150	22	5.8	none

Tungsten electrode : 2% Thoriated

WELDING TECHNIQUE (QW 410)

Single/Multi pass	: Multipass	Oscillation	: N/A
Side welded	: One	Peening	: N/A
String/Weave Bead	: Stringer	Orific size	: 10mm
Filler Added	: Added	Method of cleaning	: Grind smooth final weld
Solid/Tube wire	: Solid	Back gouging	: N/A
Tube-work distance	: 10mm	Single/Multi electrode	: Single
Electrode spacing	: N/A		

POST WELD HEAT TREATMENT (QW 407)

Heat rate	: N/A	Cool rate	: N/A
Hold temp	: N/A	Method	: N/A
Hold time	: N/A	Other	: No PWHT

Figure A.3: Modified Welding Procedure Specification (WPS) used to weld geometry 1.

Appendix B: Fatigue life calculations

B.1 Strain gage calibration

The active strain gage (R_1) was connected in a quarter wheatstone bridge configuration as described by Van Tonder (Van Tonder, 2004). This is shown in Figure B-1a) There was chosen to use a shunt resistor (R_p) to unbalance the bridge and do the calibration for the strain gage, as shown in Figure B-2b).

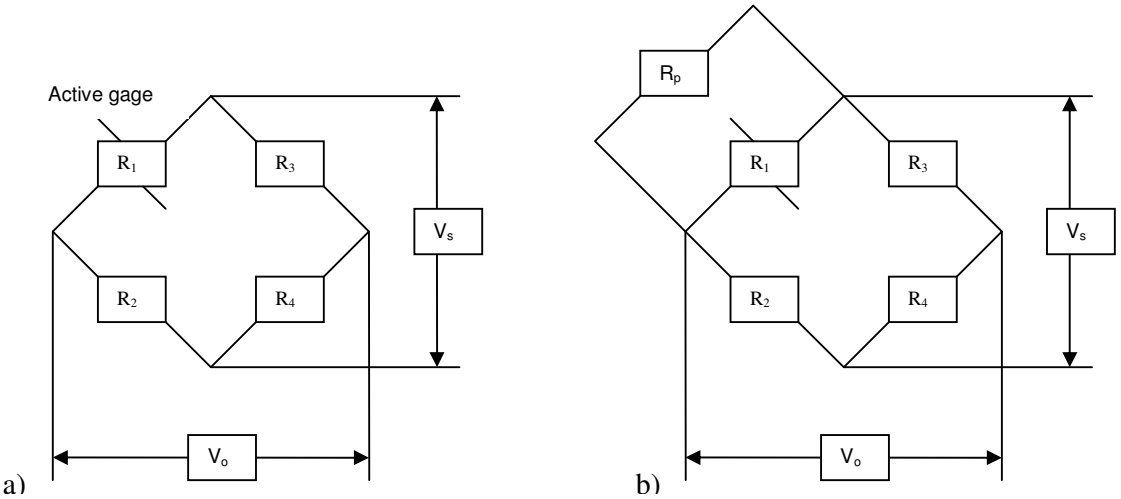

Figure B-1 Wheatstone bridge configuration used for the connection and calibration of the strain gages.

The approximate change in output voltage over input voltage can be described as:

$$\frac{V_o}{V_s} = \frac{1}{4}\left(\frac{\Delta R_1}{R_1} - \frac{\Delta R_2}{R_2} + \frac{\Delta R_3}{R_3} - \frac{\Delta R_4}{R_4}\right) \qquad (1)$$

Where

V_o = Output voltage

V_s = Input voltage

However applying the shunt resistor to the balanced Wheatstone bridge results in an unbalanced bridge represented by an quarter bridge configuration i.e. the unbalance due to the shunt resistor can be interpreted as a quarter bridge configuration. This implies that:

$$\frac{\Delta R_2}{R_2} = \frac{\Delta R_3}{R_3} = \frac{\Delta R_4}{R_4} = 0 \qquad (2)$$

By substituting equation (2) into equation (1) the change in output voltage over change in input voltage now becomes:

$$\frac{V_o}{V_s} = \frac{1}{4}\frac{\Delta R_1}{R_1} \qquad (3)$$

As the shunt resistor is connected in parallel with the strain gage equation (3) now becomes:

$$\frac{V_o}{V_s} = \frac{1}{4}\left(\frac{R_p}{R+R_p} - 1\right) \qquad (4)$$

Where

R = Strain gage resistance

R_p = Shunt resistor

However from the gage factor we know that:

$$\frac{\Delta R}{R} = k\varepsilon \qquad (5)$$

Equation (3) now becomes:

$$\frac{V_o}{V_S} = \frac{1}{4}k\varepsilon = \frac{1}{4}\left(\frac{R_p}{R+R_p} - 1\right) \qquad (6)$$

Then the strain is equal to:

$$\varepsilon = \frac{1}{k}\left(\frac{R_p}{R+R_p} - 1\right)x10^6 \quad in\mu m/m \qquad (7)$$

The strain gage properties as supplied by the manufacturer were given as follow:

Gage factor (k) = 2.01

Strain gage resistance (R) = 120.01Ω

Shunt resistor used (R_p)= 120kΩ

By using equation (7) the simulated strain can be calculated as:

$$\varepsilon = \frac{1}{k}\left(\frac{R_p}{R+R_p}-1\right)\times 10^6$$
$$= \frac{1}{2.01}\left(\frac{120000}{120.01+120000}-1\right)\times 10^6$$
$$= -497.057\mu\varepsilon$$

Using equation (6) this simulated strain should be equal to

$$\frac{V_o}{V_s} = \frac{1}{4}k\varepsilon$$
$$= \frac{1}{4}(2.01)\left(-497.057\times 10^3\right)$$
$$= -0.24977 mV/V$$

Therefore according to the calculations -0.24977mV/V is equal to -497.057με and therefore a change of 1 mV/V reading obtained on the output signal will be equal to a change in strain of 1990.06με.

For each strain gage used the shunt resistor was placed over the strain gage and a reading of 0.249mV/V was obtained. This corresponds to the calculated value above. As the measured and the calculated value correspond it can be concluded that the strain gage was adhered correctly to the test piece and that each 1 mV/V reading obtained from the strain gage will correspond to a change in strain equal to 1990.06με.

B.2 Displacement data

The displacements of the welded samples were measured after the first, second, eighth and final weld as the weld sequence presented in Figure 4-4 progressed.

All displacements were measured by placing the samples flat on a work bench. The distances to points 3 and 4 were then measured by placing a ruler 90 degrees to the workbench. Only upward displacements were measured. The distortions were measured at the location as shown in Figure 4-7.

Table B-1: Upward displacements measured during welding of the samples after weld pass 1, 2, 8 and of the final welded samples. All dimensions are in mm.

	Point 3[(1)]				Point 4[(2)]			
	After weld pass 1	After weld pass 2	After weld pass 8	Final sample	After weld pass 1	After weld pass 2	After weld pass 8	Final sample
Geometry 1								
Sample 1	4	10	14	18	n/a	101	131	122
Sample 2	5	10	15	19	n/a	100	132	122
Sample 3	5	11	15	18	n/a	100	130	123
Sample 4	5	10	16	19	n/a	100	132	122
Average	5	10	15	18.5	n/a	100	131	122
Geometry 2								
Sample 1	5	10	15	16	n/a	100	131	129
Sample 2	5	11	15	16	n/a	100	131	129
Sample 3	6	10	16	17	n/a	100	130	128
Sample 4	4	9	15	16	n/a	100	132	130
Average	5	10	15	16	n/a	100	131	129

Notes:
[(1)]Distance B, starting distance 0mm.
[(2)]Distance A, starting distance 100mm.

B.3 Nominal Stress Approach

For the nominal stress approach the head to skirt weld was classified as a full penetration T-joint, detail 411, as this is the closest geometry to the actual geometry tested. (Hobbacher, 2004:60) This gave a FAT class of 80, which means that the sample will fail after 2 million cycles if a stress range of 80 MPa is applied.

The SN-curve for predicting the fatigue life was determined as follow:

$$N = C_o \Delta\sigma^{-3}$$
$$C_o = N\Delta\sigma^3$$
$$= (2000000)(80)^3$$
$$= 1.024\times10^{12}$$

Thus

$$N = 1.024\times10^{12}\Delta\sigma^{-3}$$

For geometry 1 an improvement factor of 1.3 on stress could be taken into account as the sample was back ground. The stress amplitude for geometry 1 therefore becomes 154.5MPa.

The expected life predicted for geometry 1 is:

$$N = \left(1.024\times10^{12}\right)(146\times2)^{-3}$$
$$= 41000 cycles$$

The expected life predicted for geometry 2 is:

$$N = (1.024\times10^{12})(190\times2)^{-3}$$
$$= 18661 cycles$$

B.4 Effective notch stress approach

The SN-curve for the effective notch stress approach is based on $\Delta\delta$ = 225 MPa at 2 million cycles. (Hobbacher, 2004:80)

Therefore the SN-curve for predicting the fatigue life can be given as:

$$N = C_o\Delta\sigma^{-3}$$
$$C_o = N\Delta\sigma^3$$
$$= (2000000)(225)^3$$
$$= 2.278\times10^{13}$$

Thus

$$N = 2.278\times10^{13}\Delta\sigma^{-3}$$

For each of the FEM analysis shown in Figure 6-4 the maximum stress in the x-direction on coord 1 was read off. This is the stress that will open the crack. The results are shown in Table 6-3.

The expected life of the sample was found to be:
Geometry 1, un-deformed:

$$N = (2.278\times10^{13})(280\times2)^{-3}$$
$$= 129722 cycles$$

Geometry 1, deformed:

$$N = (2.278\times10^{13})(281\times2)^{-3}$$
$$= 128342 cycles$$

Geometry 2, un-deformed:

$$N = (2.278\times10^{13})(351\times2)^{-3}$$
$$= 65852 cycles$$

Geometry 2, deformed:

$$N = (2.278\times10^{13})(332\times2)^{-3}$$
$$= 77817 cycles$$

Appendix C: Detail drawings of weld and fatigue jig

C.1 General Arrangement – Fatigue Jig

C.2 Rigid Test Rig – Fatigue Jig

C.3 Rod End Connectors, Actuator Connection and Clamping plates – Fatigue Jig

C.4 General Arrangement – Weld Jig

C.5 Solid Weld Jig

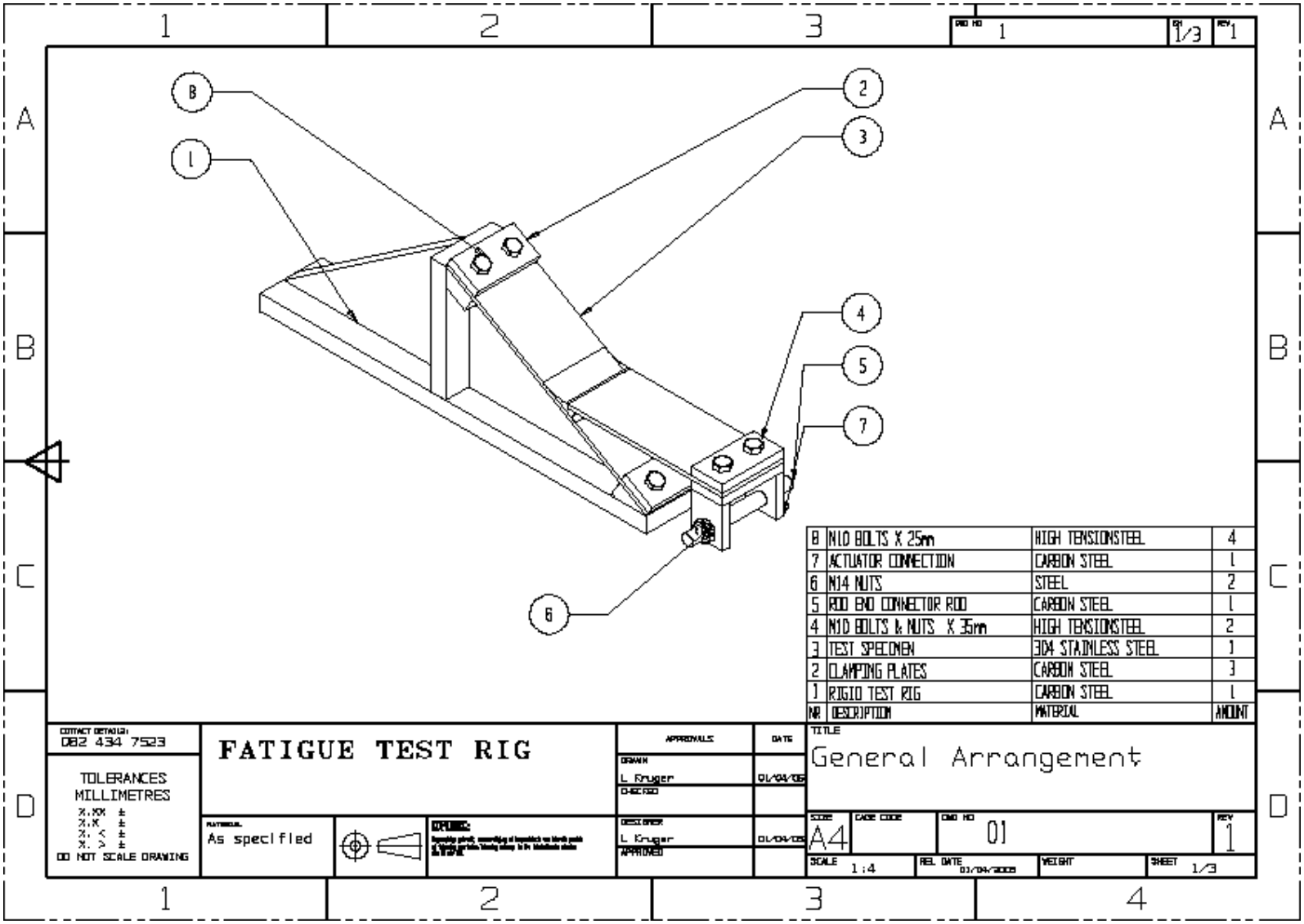
DWG NO 1
SH 1/3
REV 1
8
7
6
5
4
3
2
1
8 M10 BOLTS X 25mm HIGH TENSIONSTEEL 4
7 ACTUATOR CONNECTION CARBON STEEL 1
6 M14 NUTS STEEL 2
5 ROD END CONNECTOR ROD CARBON STEEL 1
4 M10 BOLTS & NUTS X 35mm HIGH TENSIONSTEEL 2
3 TEST SPECIMEN 304 STAINLESS STEEL 1
2 CLAMPING PLATES CARBON STEEL 3
1 RIGID TEST RIG CARBON STEEL 1
NR DESCRIPTION MATERIAL AMOUNT
CONTACT DETAILS: 082 434 7523
FATIGUE TEST RIG
APPROVALS
DATE
DRAWN L Kruger 01/04/05
CHECKED
DESIGNER L Kruger 01/04/05
APPROVED
TOLERANCES MILLIMETRES
X.XX ±
X.X ±
X. < ±
X. > ±
DO NOT SCALE DRAWING
MATERIAL As specified
TITLE General Arrangement
SIZE A4
CAGE CODE
DWG NO 01
REV 1
SCALE 1:4
REL DATE 01/04/2005
WEIGHT
SHEET 1/3

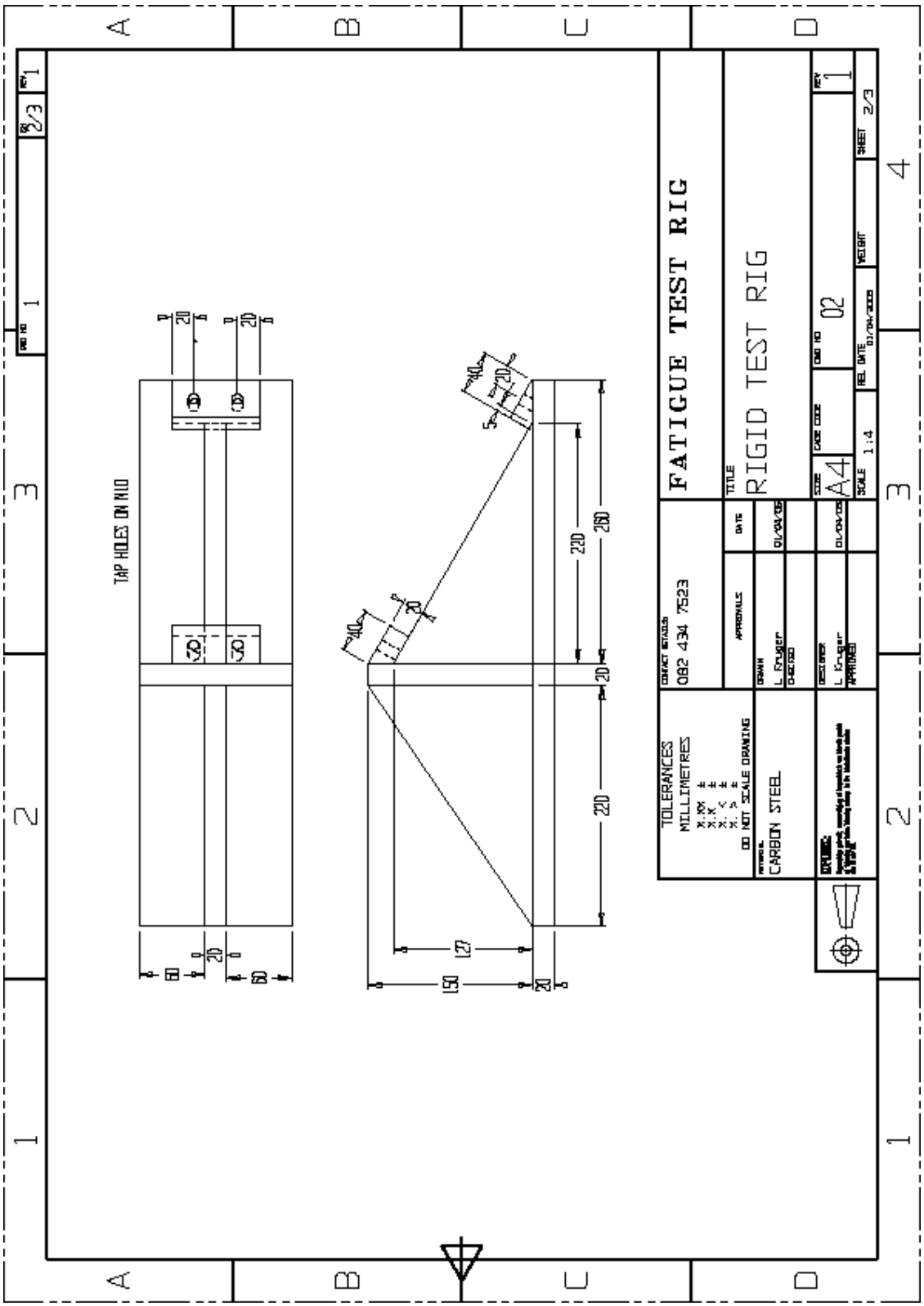
FATIGUE TEST RIG
RIGID TEST RIG
TAP HOLES ON M10
CARBON STEEL
DO NOT SCALE DRAWING
TOLERANCES
MILLIMETRES
A4
SCALE 1:4
SHEET 2/3
220
260
150
127
20
40
60

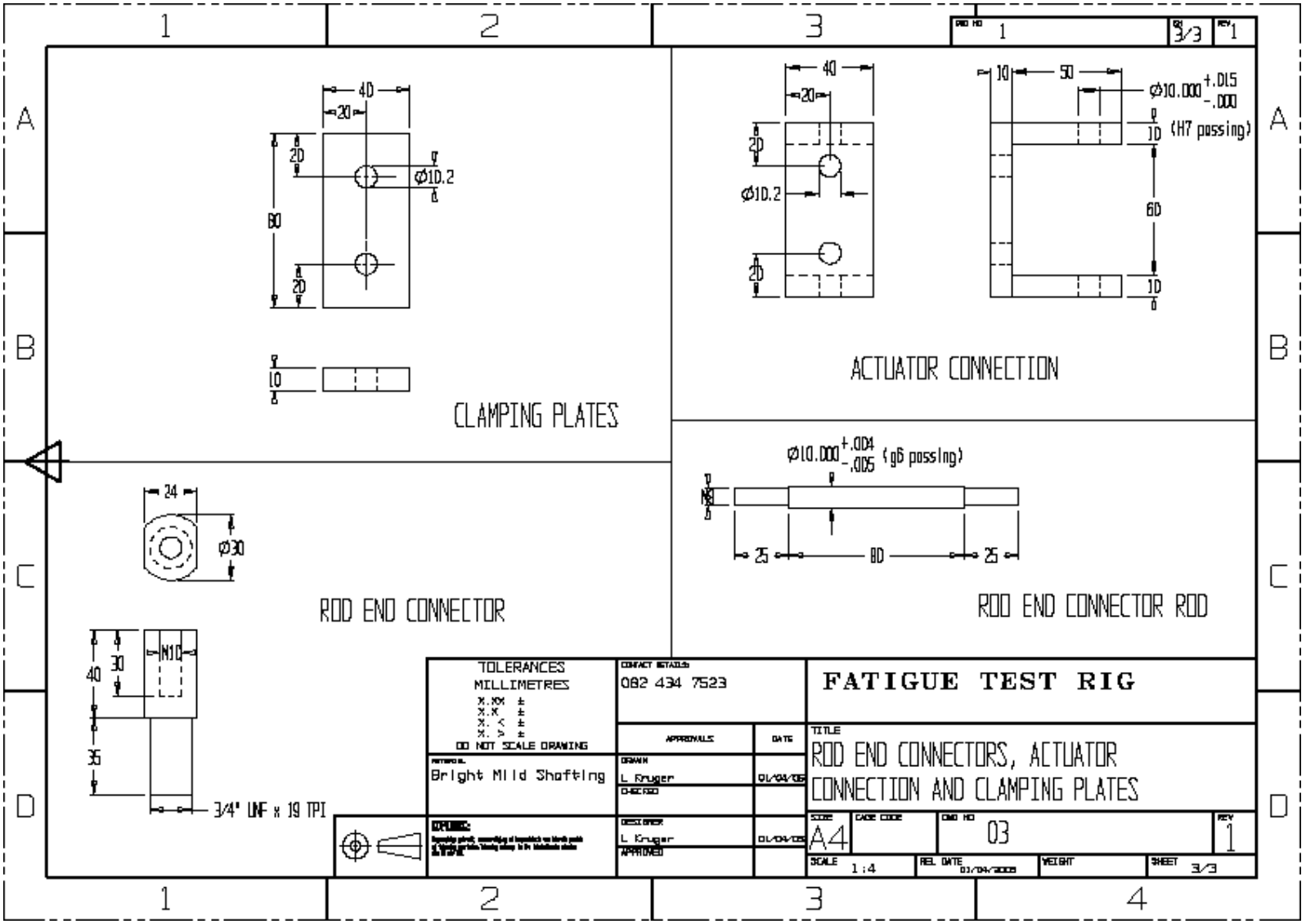
1
2
3
4
A
B
C
D
DWG NO 1
SH 3/3
REV 1
40
20
2D
Ø10.2
80
10
CLAMPING PLATES
ACTUATOR CONNECTION
50
Ø10.000 +.015 -.000 (H7 passing)
60
Ø10.000 +.004 -.005 (g6 passing)
25
80
ROD END CONNECTOR ROD
24
Ø30
ROD END CONNECTOR
M10
30
35
3/4" UNF x 19 TPI
TOLERANCES
MILLIMETRES
X.XX ±
X.X ±
X. < ±
X. > ±
DO NOT SCALE DRAWING
CONTACT DETAILS
082 434 7523
APPROVALS
DATE
Bright Mild Shafting
DRAWN
L Kruger
01/04/05
CHECKED
DESIGNED
L Kruger
01/04/05
APPROVED
FATIGUE TEST RIG
TITLE
ROD END CONNECTORS, ACTUATOR CONNECTION AND CLAMPING PLATES
SIZE A4
CAGE CODE
DWG NO 03
REV 1
SCALE 1:4
REL DATE 01/04/2005
WEIGHT
SHEET 3/3

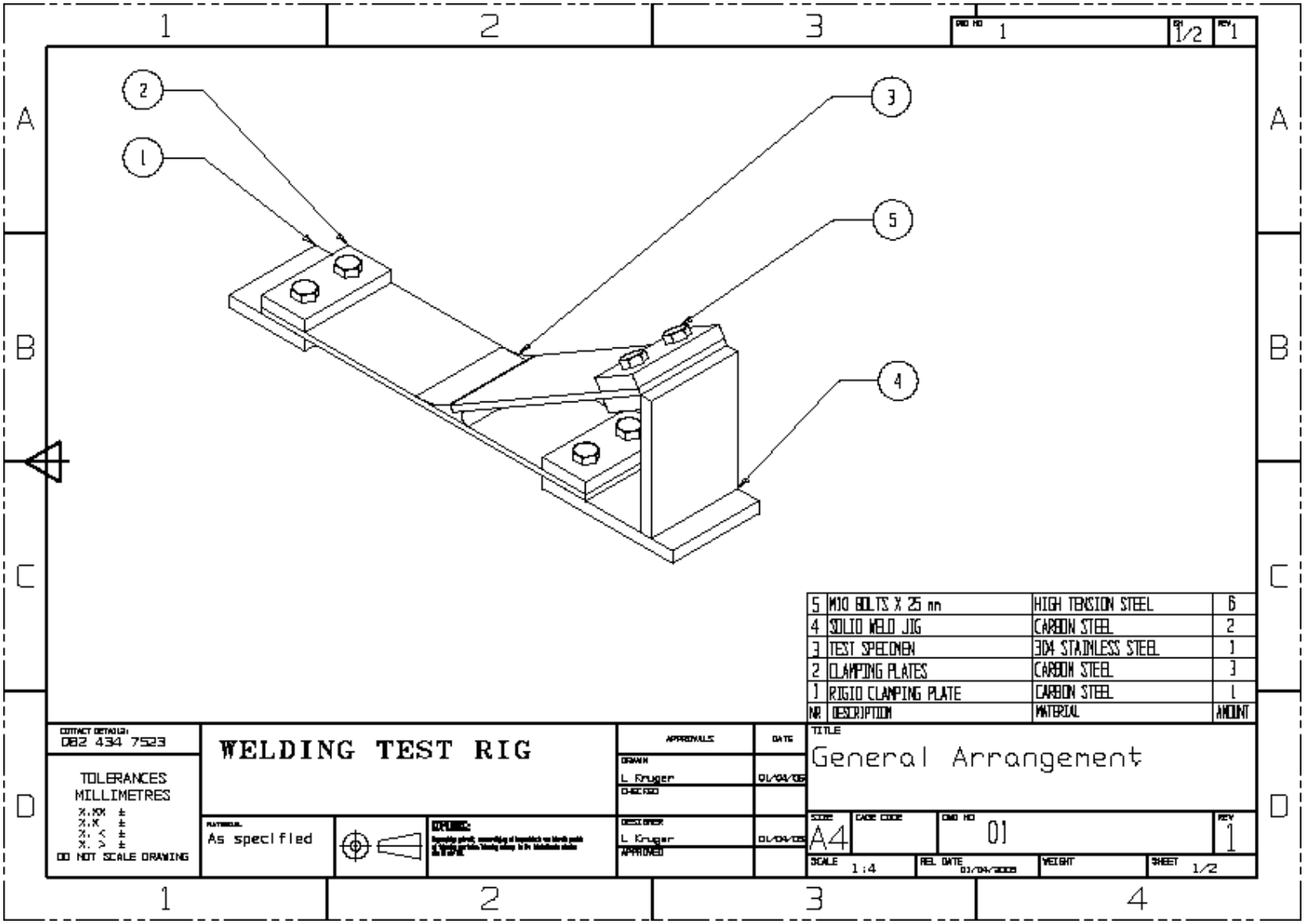
1
2
3
DWG NO 1
SH 1/2
REV 1
A
B
C
D
2
1
3
5
4
5 M10 BOLTS X 25 mm HIGH TENSION STEEL 6
4 SOLID WELD JIG CARBON STEEL 2
3 TEST SPECIMEN 304 STAINLESS STEEL 1
2 CLAMPING PLATES CARBON STEEL 3
1 RIGID CLAMPING PLATE CARBON STEEL 1
NR DESCRIPTION MATERIAL AMOUNT
CONTACT DETAILS: 082 434 7523
TOLERANCES MILLIMETRES
X.XX ±
X.X ±
X. < ±
X. > ±
DO NOT SCALE DRAWING
WELDING TEST RIG
MATERIAL As specified
APPROVALS DATE
DRAWN L Kruger 01/04/05
CHECKED
DESIGNER L Kruger 01/04/05
APPROVED
TITLE General Arrangement
SIZE A4
CAGE CODE
DWG NO 01
REV 1
SCALE 1:4
REL DATE 01/04/2005
WEIGHT
SHEET 1/2

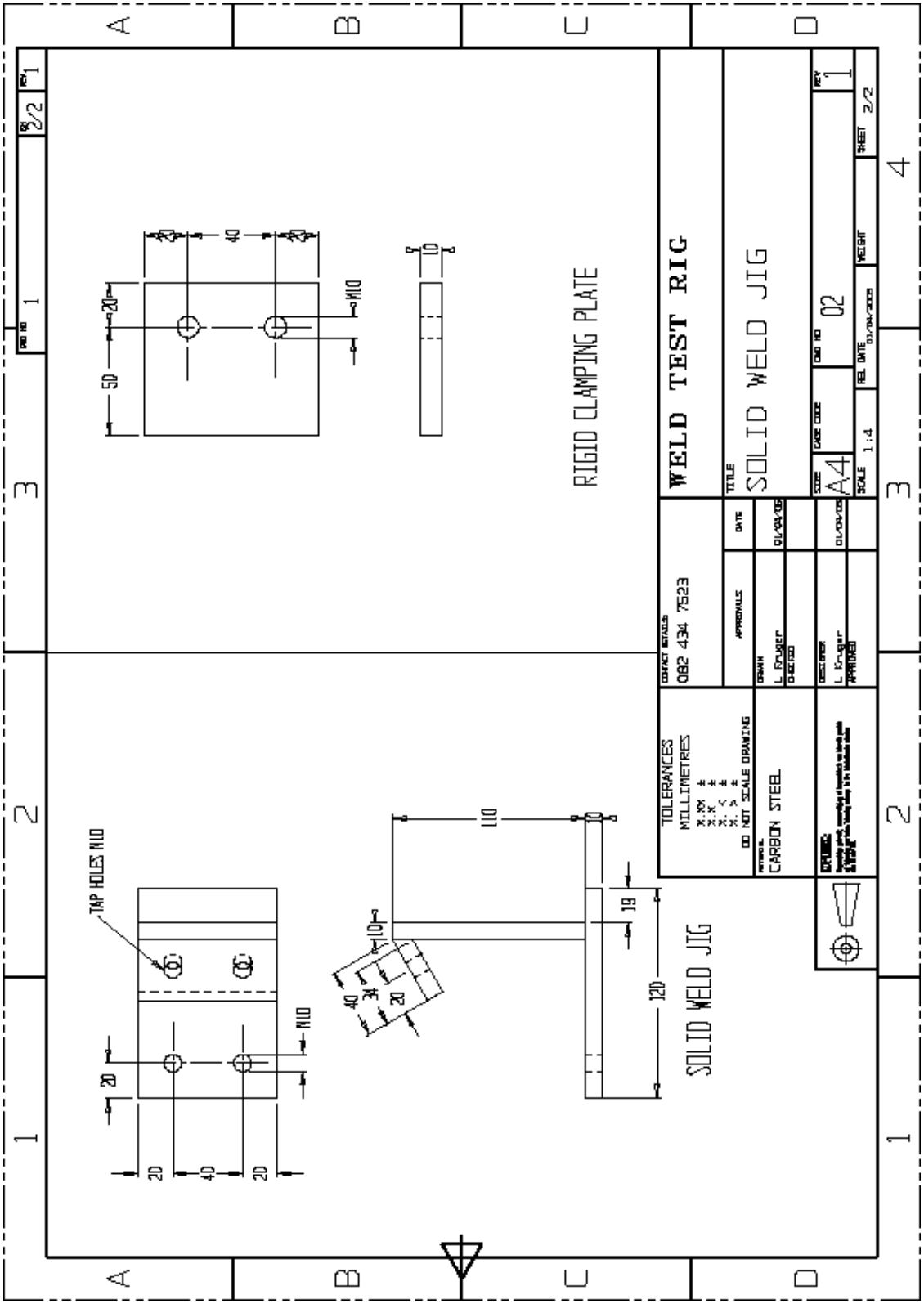
RIGID CLAMPING PLATE
SOLID WELD JIG
TAP HOLES M10
WELD TEST RIG
SOLID WELD JIG
TOLERANCES
MILLIMETRES
DO NOT SCALE DRAWING
CARBON STEEL
A4
SCALE 1:4
SHEET 2/2

Appendix D: Rod End Data

PTI

Rod ends GAR..DO
requiring maintenance, right hand thread
(GAR..ES)

Part No.	Dimensions (mm)															kg	Dyn. (N)	Static (N)
	d	d_2	l_2	Alpha	B	C_1	D	d_1	d_3	d_5	h	h_1	h_2	$r_{1s\,min}$	$RALU_{max}$	$RALU_{min}$	m	C_r	C_{0r}
GAR 6 DO	6	21	48,5	13	6	4,4	14	8	M8	10	36	18	12	0,3	0,068	0,023	0,017	3400	6920
GAR 8 DO	8	24	54	15	8	6	16	10,2	M8	13	42	22	14	0,3	0,068	0,023	0,029	5500	12900
GAR 10 DO	10	29	62,5	12	9	7	19	13,2	M10	16	48	26	15	0,3	0,068	0,023	0,051	8150	20600
GAR 12 DO	12	34	71	11	10	8	22	14,9	M12	19	54	28	18	0,3	0,068	0,023	0,085	10800	30100
GAR 15 DO	15	40	83	8	12	10	26	18,4	M14	22	63	34	20	0,3	0,092	0,03	0,14	17000	41500
GAR 17 DO	17	46	92	10	14	11	30	20,7	M16	25	69	36	23	0,3	0,092	0,03	0,19	21200	56500
GAR 20 DO	20	53	104,5	9	16	13	35	24,1	M20x1,5	29	78	43	27	0,3	0,092	0,03	0,31	30000	75600
GAR 25 DO	25	64	126	7	20	17	42	29,3	M24x2	35,5	94	53	32	0,6	0,1	0,037	0,56	48000	99200
GAR 30 DO	30	73	146,5	6	22	21	47	34,2	M30x2	40,7	110	65	37	0,6	0,1	0,037	0,89	62000	119000

Appendix E: Strain Gage Data

SG / Y series with 1 measuring grid / linear strain gages

Stock types: Steel	Aluminum	Others	Variants: Nominal resistance Ω	Dimensions (mm) [1 inch = 25.4 mm] Measuring grid a	b	Measuring grid carrier c	d	Max. perm. effective bridge excitation voltage V	Solder terminals
1-LY11-0.6/120	1-LY13-0.6/120	1-LY1x-0.6/120#	120	0.6	1	5	3.2	1.5	LS 7
1-LY11-1.5/120	1-LY13-1.5/120	1-LY1x-1.5/120	120	1.5	1.2	6.5	4.7	2.5	LS 7
1-LY11-3/120	1-LY13-3/120	1-LY1x-3/120	120	3	1.4	8.5	4.5	4	LS 7
1-LY11-3/120A		1-LY1x-3/120A	120	3	1.4	8.5	4.5	4	LS 7
1-LY11-6/120	1-LY13-6/120	1-LY1x-6/120	120	6	2.8	13	6	8	LS 5
1-LY11-6/120A		1-LY1x-6/120A	120	6	2.8	13	6	8	LS 5
1-LY11-10/120	1-LY13-10/120	1-LY1x-10/120	120	10	4.9	18.5	9.5	13	LS 5
1-LY11-10/120A		1-LY1x-10/120A	120	10	4.9	18.5	9.5	13	LS 5
1-LY11-1.5/350	1-LY13-1.5/350	1-LY1x-1.5/350#	350	1.5	1.2	5.7	4.7	4.5	LS 7
1-LY11-3/350	1-LY13-3/350	1-LY1x-3/350	350	3	1.5	8.5	4.5	7	LS 7
		1-LY1x-3/350A	350	3	1.5	8.5	4.5	7	LS 7
1-LY11-6/350	1-LY13-6/350	1-LY1x-6/350	350	6	2.9	13	6	14	LS 5
1-LY11-6/350A		1-LY1x-6/350A	350	6	2.9	13	6	14	LS 5
1-LY11-10/350		1-LY1x-10/350	350	10	5	18.5	9.5	23	LS 5
1-LY11-10/350A		1-LY1x-10/350A	350	10	5	18.5	9.5	23	LS 5

LY11

Linear strain gage
Temperature response matched to steel with α_t = 10.8 · 10⁻⁶/K

LY13

Temperature response matched to aluminum with α_t = 23 · 10⁻⁶/K

LY1x

Temperature response matching at customer's choice, see page 20

Illustrations show actual size
(Grid length in mm)

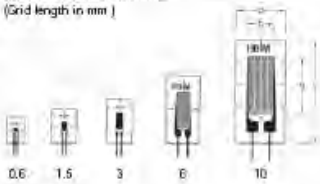

Contents per package: 10 pcs.

Stock types: Steel	Aluminum	Others	Variants: Nominal resistance Ω	Dimensions (mm) [1 inch = 25.4 mm] Measuring grid a	b	Measuring grid carrier c	d	Max. perm. effective bridge excitation voltage V	Solder terminals
1-LY21-0.6/120		1-LY2x-0.6/120#	120	0.6	0.8	3.5	6.4	1	LS 7
1-LY21-1.5/120		1-LY2x-1.5/120	120	1.5	1.4	4.7	8.3	2	LS 5
1-LY21-3/120		1-LY2x-3/120	120	3	2.8	7.5	10	6	LS 5
		1-LY2x-6/120	120	6	5.7	11	16	12	LS 4

Types marked # are only available with matching to aluminum, ferritic or austenitic steel

LY21

Linear strain gage
Temperature response matched to steel with α_t = 10.8 · 10⁻⁶/K

LY2x

Temperature response matching at customer's choice, see page 20

Illustrations show actual size
(Grid length in mm)

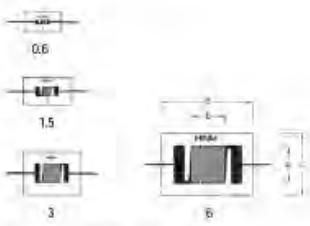

Contents per package: 10 pcs.

Appendix F: Flow diagrams of procedure followed during welding and fatigue testing

F.1 Procedure followed during fatigue testing